

# Spinal Cord Regeneration via Collagen Entubulation

by

Sajjad S. Matin

B.S., Biomedical Engineering  
B.S., Materials Science and Engineering  
The Johns Hopkins University, 2001

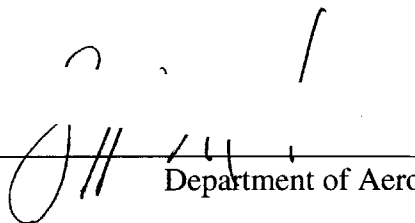
Submitted to the Department of Aeronautics and Astronautics  
in Partial Fulfillment of the Requirements for the  
Degree of

Master of Science in Aeronautics and Astronautics

at the  
Massachusetts Institute of Technology  
September 2004

© 2004 Massachusetts Institute of Technology  
All Rights Reserved

Signature of Author \_\_\_\_\_



Department of Aeronautics and Astronautics  
August 19, 2004

Certified by \_\_\_\_\_

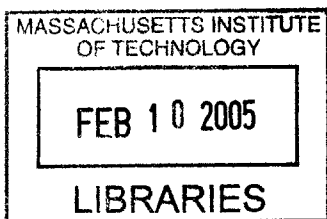


Myron Spector  
Senior Lecturer, Department of Mechanical Engineering, MIT  
Professor of Orthopedic Surgery (Biomaterials), HMS

Accepted by \_\_\_\_\_



Jaime Peraire  
Professor of Aeronautics and Astronautics  
Chair, Committee on Graduate Students



AERO 13

# **Spinal Cord Regeneration via Collagen Entubulation**

by

Sajjad S. Matin

Submitted to the Department of Aeronautics & Astronautics  
on August 20, 2004, in Partial Fulfillment of the  
Requirements for the Degree of  
Master of Science in Aeronautics & Astronautics

## **Abstract**

Traumatic injury to the adult mammalian spinal cord results in varying degrees of lost motor and sensory nerve function. Damaged axons of the central nervous system (CNS) exhibit a severely limited regenerative capacity; paralysis induced by severe trauma is generally permanent. Previous studies have attempted to simulate the peripheral nerve environment, where axonal regeneration is spontaneous, through the implantation of peripheral nerve graft tissue, exogenous growth factors or prosthetic devices. Such intervention has demonstrated the ability of central nerve axons to regrow over significant distances and partially restore distal limb function.

The current work aims at evaluating the efficacy of two distinct collagen implants towards promoting spinal cord regeneration. The experimental spinal lesion is a 5mm mid-thoracic gap created by transections at T7 and T9 and removal of intermediary cord and peripheral roots. The two implants offered different entubulation schemes; one implant was a thin walled tube composed of Type I bovine collagen, the other a commercially available bilayered membrane composed of Types I and III porcine collagen. Whereas the tube was fitted directly into the spinal lesion, the membrane was wrapped around the cord stumps like a tubular bandage. Five experimental groups defined the current research: Groups I and II received no implant, Groups III and IV were implanted with tubes, and Group V was implanted with the membrane wrap. A secondary aim of the research was to validate the use of a dorsal barrier in further reducing scar infiltration to the wound. This additional collagen membrane was simply draped over the implant (or lesion) of Groups II, IV and V.

Mid-thoracic spinal cord sections were explanted from all groups 4 weeks (28 days) post-implantation. Histological and immunohistochemical analyses showed severe fibrous and glial scar formation in Groups I and III, less fibrous scarring in Group II and very little scar manifesting in Groups IV and V. A quantitative analysis of myelinated axons in the center of the explants corresponded with the assessment of scar as a physical barrier to competent axon growth. Groups I and III exhibited the least regenerated axons, Groups IV and V the most. The findings also validated the effectiveness of the dorsal barrier in promoting spinal cord regeneration.

Overall, the combination of wrap membrane and dorsal barrier (Group V) proved most effective in creating a hospitable environment for regenerative success.

Thesis Supervisor: Myron Spector  
Title: Senior Lecturer, Department of Mechanical Engineering, MIT  
Professor of Orthopedic Surgery (Biomaterials), HMS

## Acknowledgements

As in any undertaking, this research was the result of a large collaborative effort. The experience and guidance of so many people, in so many varying fields, contributed immeasurably towards the completion of this paper; I only fear that words alone can not capture my gratitude (but until someone perfects holography, words will have to do).

I would like to thank Dr. Spector for serving as my research advisor and mentor. I have learned a great deal in his lab and classes and have always appreciated his insights and advice. I am also a big fan of his semi-*laissez faire* policies, where I was given enough latitude to appreciate the research for its greater goals.

I am indebted to the surgical expertise of Dr. Hu-Ping Hsu. I know enough about doctors to appreciate when one doesn't get mad that non-sterile hands accidentally touched sterile instruments during a surgery. Similarly, I am grateful for the patience and devotion of Diane Ghera and Dr. Arthur Nedder, of the VA Animal Research Facility, towards the welfare of all animals (including my rats).

I would like to thank Camille Francois, Dr. Erika Marsilio and all the members of the Tissue Engineering Lab and Orthopedic Research Lab for their helpful advice, time and expertise. I am grateful for the opportunity to work with Dr. Yannas and have always admired his sincere professionalism. The learning curve for the current research was immensely shortened by the guidance and resourcefulness of Brendan Harley (much to his chagrin); I am grateful for all his help.

I would also like to thank Dr. Dava Newman, my academic advisor, and everyone at the Man-Vehicle Lab for easing my transition into the graduate world. Dava remains the only person never to have asked what the spinal cord has to do with outer space\* – for that I am extremely grateful.

More personally, I am ever deferent to Allah and his messenger, a little less so to my parents (for whom this paper is validation that I did something productive in Boston), and strikingly irreverent to my older sister and brother. I am grateful for having a family that supports my interests and friends that provide me with new ones.

---

\* see Section 1.7

## Table of Contents

Abstract.....	2
Acknowledgements.....	3
Table of Contents.....	4
List of Figures.....	6
List of Tables.....	7
<b>Chapter 1: Introduction.....</b>	<b>8</b>
1.1 Problem Statement.....	8
1.2 The Nervous System.....	8
1.2.1 <i>The Neuroglia</i> .....	8
1.2.2 <i>The Neuron</i> .....	9
1.2.3 Basic Anatomy of the Spinal Cord.....	10
1.3 Injury to the Peripheral Nervous System.....	10
1.4 Injury to the Central Nervous System.....	11
1.5 Current and future progress in treating Spinal Cord Injury (SCI).....	12
1.6 Objectives of the Current Research.....	14
1.7 Relevance of Current Study to the field of Aeronautics and Astronautics....	15
<b>Chapter 2: Materials.....</b>	<b>16</b>
2.1 Rationale for current material selection.....	16
2.2 Materials Preparation.....	16
2.2.1 <i>Type I collagen tube</i> .....	16
2.2.2 <i>BioGide® collagen membrane</i> .....	17
2.3 Material Characteristics.....	18
2.4 Results.....	20
2.4.1 <i>Average Pore Diameter</i> .....	20
2.4.2 <i>Average Porosity</i> .....	20
2.5 Discussion.....	21
<b>Chapter 3: Methods.....</b>	<b>24</b>
3.1 Injury Model.....	24
3.2 Animal Model.....	24
3.3 Animal Sacrifice.....	29
3.4 Tissue Retrieval and Processing.....	29
3.4.1 <i>Rostral Segment</i> .....	30
3.4.2 <i>Caudal Segment</i> .....	31
<b>Chapter 4: Results.....</b>	<b>33</b>
4.1 General Observations.....	33
4.2 Morphological Observations.....	33
4.3 Observations from Histology.....	35
4.4 Observations from Immunohistochemistry.....	38
4.5 Axonal Regeneration.....	39

<b>Chapter 5: Discussion.....</b>	<b>44</b>
<b>Chapter 6: Conclusions.....</b>	<b>47</b>
<b>Appendix A: 5% Collagen Tube Fabrication Protocol.....</b>	<b>48</b>
<b>Appendix B: The Teflon Mold.....</b>	<b>50</b>
<b>References.....</b>	<b>51</b>
Works cited.....	51
Sources for certain figures.....	57

## List of Figures

Figure 1.1	Illustration of the neuron.....	9
Figure 1.2	Basic anatomy of the spinal cord.....	10
Figure 1.3	Regeneration in the peripheral nervous system.....	11
Figure 2.1	Low magnification image of the BioGide® membrane stained to show collagen structure.....	19
Figure 2.2	Low magnification image of the 5% (w/w) collagen tube stained to show collagen structure.....	19
Figure 3.1	Illustration of the implants within the five different experimental groups.....	26
Figure 3.2	Surgical Image: Laminectomy.....	28
Figure 3.3	Surgical Image: Transections at T7 and T9.....	28
Figure 3.4	Surgical Image: Removal of transected tissue and creation of the gap lesion.....	28
Figure 3.5	Surgical Image: Implantation of the collagen tube.....	28
Figure 3.6	Surgical Image: Completed tube implantation.....	28
Figure 3.7	Surgical Image: BioGide® membrane insertion into the lesion.....	29
Figure 3.8	Surgical Image: Entubulation of the lesion by the membrane.....	29
Figure 3.9	Surgical Image: Placement of the dorsal barrier over the wrap implant.....	29
Figure 3.10	Image of the explanted cord, 4 weeks post-implantation, from Group V.....	30
Figure 4.1	Low magnification image of an H&E stained cross-section of a Group V explant.....	34
Figure 4.2	Low magnification image of an H&E stained cross-section of a Group IV explant.....	34
Figure 4.3	Dense, crimped collagen formation in the lesion of a Group II explant.....	37
Figure 4.4	Loose collagen formation in the lesion of a Group V explant.....	37
Figure 4.5	Coherent formation of a tissue/implant interface for a Group V explant.....	37
Figure 4.6	The lack of a tissue/implant interface in a Group III explant.....	37
Figure 4.7	SMA infiltration and fibrous scar in a Group II explant.....	38
Figure 4.8	Image of myelinated axons, stained dark blue, regenerated across the lesion.....	39
Figure 4.9	Number of myelinated axons in the center of the lesion for all experimental groups.....	40
Figure 4.10	Axon Diameter Distribution: Group I.....	41
Figure 4.11	Axon Diameter Distribution: Group II.....	42
Figure 4.12	Axon Diameter Distribution: Group III.....	42
Figure 4.13	Axon Diameter Distribution: Group IV.....	43
Figure 4.14	Axon Diameter Distribution: Group V.....	43
Figure B.1	Image of the Teflon mold.....	50
Figure B.2	Image of the Teflon mold with Teflon coated mandrel.....	50

## List of Tables

Table 2A	Measured hydraulic pore diameters of collagen implants.....	20
Table 2B	Measured porosities of collagen implants.....	20
Table 3A	List of Experimental Groups.....	26
Table 4A	Experimental groups and the number of rats within each.....	33
Table 4B	A summary of the general morphology of regrown spinal cord tissue cross-sections.....	35

## **Chapter 1: Introduction**

### **1.1 Problem Statement**

Spinal cord injuries (SCI) afflict roughly 10,000 Americans each year with a prevalence of over 200,000 people living with related trauma. It is estimated that by 2005 nearly 500,000 new cases will increase the total world population of people living with SCI induced paralysis to over 2.5 million. (ICCP 2000) Unlike the peripheral nervous system (PNS), spontaneous axonal regeneration and functional rehabilitation are rarely initiated following injury of the central nervous system (CNS).

Current clinical management of SCI involves stabilization of the spine, reduction of inflammatory and immunological responses and early rehabilitative therapy. Although such intervention reduces inflammation and the concomitant effects of cellular damage and cyst formation, it does not attempt to promote full functional rehabilitation via nerve regeneration. The regeneration of damaged axons to their target sites affords a cogent means of recovering motor and sensory function in distal limbs.

### **1.2 The Nervous System**

The nervous system provides an intricate network for communication between the host organism's internal and external environments. Sensory perception, integrative processing and motor control are linked by specialized components within this system. The transmission, reception and propagation of electrochemical signals are conducted over varying distances by neurons. Other cells, the neuroglia, serve ancillary roles in support of proper neuronal function.

#### ***1.2.1 The Neuroglia***

The neuroglia, or glia, while not actively engaged in signal transduction, provide the neuron with an environment where communication is possible and expedient. Schwann cells, glial cells of the PNS, ensheath axons in an insulative lipoprotein called myelin. Myelinated axons are able to conduct signal impulses at significantly greater speeds than unmyelinated axons. Myelination of axons in the CNS is provided by oligodendroglia. The Schwann cells of the PNS have an intimate relationship with their axonal environment; a single cell will only



ensheath itself around a portion of a single axon, with the length of the axon myelinated by a series of Schwann cells. This is in contrast to the oligodendroglia of the CNS which extend myelinating covers to many axons simultaneously.

Another prominent glial cell of the CNS is the astrocyte, which regulates the local neural environment and isolates adjacent axon synapses from each other to promote coherent signal transduction.

### 1.2.2 The Neuron

Typically, a neuron consists of a cell body, or soma, dendrites and an axon (Figure 1.1) The soma, containing the cell nucleus, is responsible for meeting the metabolic demands of the neuron. Dendrites are branchlike extensions from the surface of the soma which serve

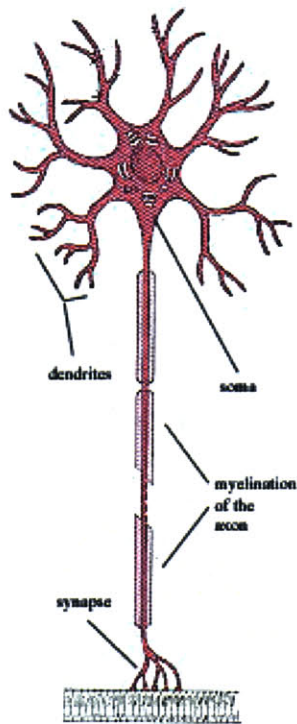


**Figure 1.1** – The neuron.

as signal reception points. The transduction of a signal from one neuron to another is facilitated via the axon, a long cable-like projection of the soma. The wide variety of functions performed by the nervous system provide for an equally diverse morphology of neurons throughout the host organism. Two such classifications, peripheral and central, are important to the current research.

The peripheral nervous system (PNS) is composed of bundles of axons which transfer signals between the external environment (or internal extremities in contact with the external environment) and the higher order processes of the central nervous system (CNS). The CNS is composed of the spinal cord and brain, both of which contain neurons that gather information from the PNS. The processed information may then be relayed back to the PNS to effect a reflex or voluntary motor function.

The morphological differences between these two neurons, those of the periphery and the central, do not affect the basic biochemical propagation of signal impulses. The differences, however, do provide highly different healing and regeneration schema amongst the two moieties. The current research is primarily concerned with injury to the CNS, i.e. the spinal cord.

### 1.2.3 Basic Anatomy of the Spinal Cord

The spinal cord is the most caudal portion of the CNS. Enclosed in the vertebral column, the cord extends from the base of the skull down to the lumbar region. The

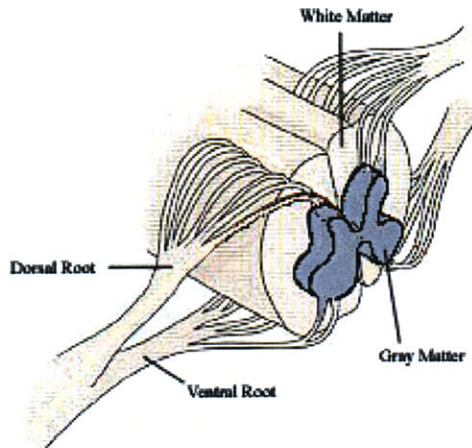


**Figure 1.2** – An exposed cross-section of the spinal cord.

interior of the cord is composed of gray matter, where the cell bodies of nerves are housed. The gray matter is surrounded by a layer of white matter composed of longitudinal tracts of myelinated axons. These axons compose the ascending and descending neural pathways through which information and commands are carried to and from the brain. The PNS and CNS are linked via sets of nerve roots, or bundled nerve fibers, which emerge in pairs along the length of the cord. As illustrated in Figure 1.2, dorsal roots

carry sensory information into the spinal cord while ventral roots send outgoing commands for motor neuron and muscle innervation. (Kandel 2000)

### 1.3 Injury to the Peripheral Nervous System

Damage to the nervous system depends on the severity and type of insult. Although complete axonal transection, or axotomy, is clinically rare it is an important experimental model with strong correlations to the more prevalent insults of blunt trauma, compression and ischemia. (Sofroniew 1999) The axon segment distal to the site of axotomy is unable to maintain its metabolic capacity; signal transmission fails immediately and is gradually followed by physical degeneration. (Kandel 2000) Without coherent signaling, the myelin sheath of the distal axon fragments and, along with the distal axon, is removed via phagocytic cells. This process of Wallerian degeneration occurs over a period of four to five days post-insult, with the axon debris removed within 48 hours. (Liu 1981)

The degeneration of the distal axon and myelin leave hollow tubes of basal lamina and their native Schwann cells. The proximal portion of the axon, still connected to the cell body, begins to regenerate outward and is attracted by chemotropic factors secreted by Schwann cells towards the remaining hollow tubes. (Grill 1999) The axons grow through the distal

tubes, becoming myelinated by the surrounding Schwann cells, and eventually reinnervate their targets. Figure 1.3 illustrates the key aspects of this regenerative process.

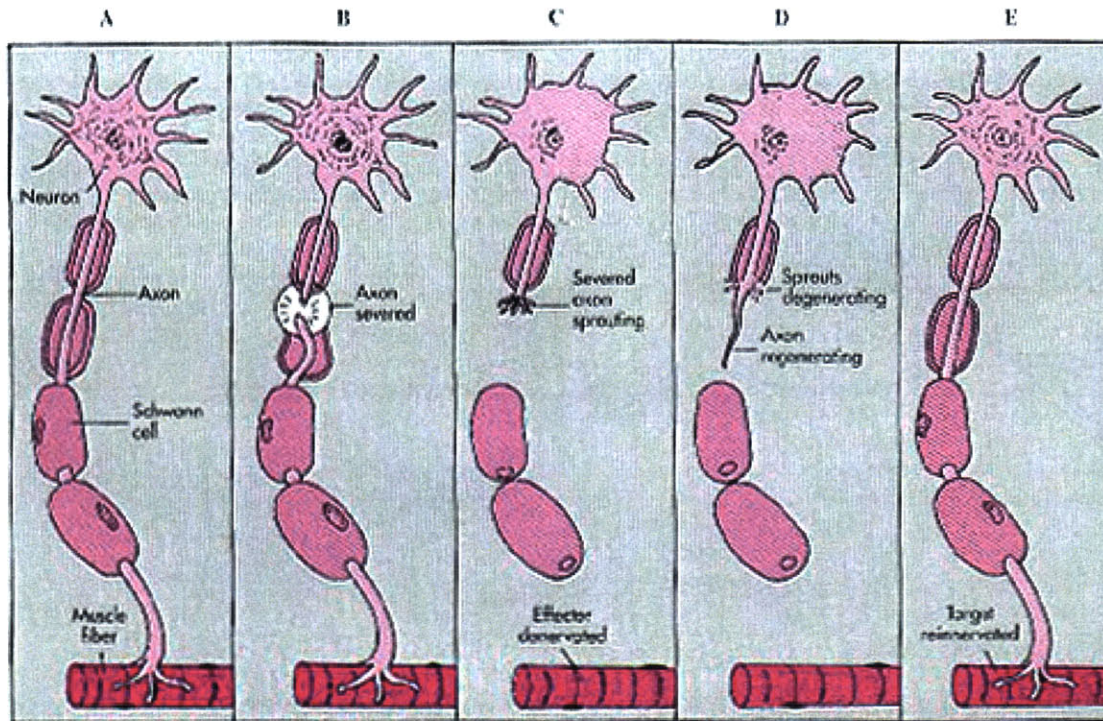


**Figure 1.3** – (A) The normal anatomy of a neuron. (B) Following transection, the target cell loses innervation and Wallerian degeneration begins. (C) The axonal growth cone begins sprouting. (D) Peripheral nerve regeneration is mediated by the presence of Schwann cells. (E) Upon completion of successful regeneration the target cell becomes reinnervated.

### 1.4 Injury to the Central Nervous System

Although a small degree of sprouting occurs from the proximal stump of the axotomized central neuron, notable axonal regeneration within the CNS is limited following injury. (Ramon y Cajal 1928) This failure is influenced by environmental factors rather than by possible limitations to regeneration intrinsic to mature central axons.

Immediately following trauma to the spinal cord, the insult is filled with blood. Blood-borne macrophages, as well as native microglia, begin to phagocytose the remnant debris. The infiltration of fibroblasts from surrounding tissue leads to the formation of densely packed connective tissue. The resulting fibrous scar poses a well studied mechanical barrier. (Windle 1950; Clemente 1954)

Inflammation, free-radical formation and excitotoxicity pose detrimental secondary damage to neurons and surrounding glia. (Blesch 2002) The resulting cyst formation and the abnormal proliferation of astrocytes, or glial scar, pose additional barriers to competent axonal growth. (Rudge 1989; Smith 1990) These reactive astrocytes have been shown to inhibit axon growth by more than just mechanical impedance. Molecules produced by astrocytes, including certain proteoglycans and tenascin, have been implicated in the failure of mature axon regeneration. (Davies 1997; Fitch 1999)

Further, the glia of the CNS are organized differently than in the PNS. Unlike the residual hollow tubes provided by Schwann cell activity in the PNS, oligodendrocytes do not offer structural guidance for coherent neurite outgrowth. (Grill 1999)

Following these stages of spinal cord injury and inflammation, further hindrance to CNS regeneration occurs by growth inhibitors within the cord's environment. (Schwab 1988; Savio 1989; Vacanti 2001; Wickelgren 2002) These molecules, associated with myelin, astrocytes and even the extracellular matrix, are believed to actively inhibit axonal regeneration as a means to control the developmental growth of the CNS. Any successful intervention to SCI must address these inhibitory signals as well as the early phases of injury.

### **1.5 Current and future progress in treating Spinal Cord Injury (SCI)**

The first pharmaceutical intervention to SCI came through the use of methylprednisolone. Proper treatment requires immediate administration of high doses directly into the lesion. This clinical intervention aims not at regenerating the cord but at reducing the devastating effects of secondary trauma induced by inflammation and free-radical formation. The preservation of nervous tissue and improved axonal response which result may be linked to the decrease in microglia and macrophage activity mediated by methylprednisolone administration. (Chen 1996; Oudega 1999) Future pharmacological intervention must address the preservation of axons, neuronal and glial cells while actively inhibiting scar formation. The use of chondroitinase ABC to cleave the glycoproteins of the glial scar has been shown to improve nerve fiber regeneration and promote motor skill rehabilitation when compared to control studies in rats with partial spinal cord transection. (Wickelgren 2002)

Classic studies by Aguayo and colleagues demonstrated that a segment of peripheral nerve grafted into a spinal cord lesion supported the regrowth of CNS axons over significant distances. (David 1981) Peripheral nerve grafts provide a substrate of extracellular matrix containing binding sites for the attachment and advancement of axon growth cones. More recent studies have worked to show the efficacy of augmenting neurotrophic factor (NTF) levels towards enhancing the regenerative response into the graft. The ability to genetically modify cellular vectors, e.g. viral, fibroblasts, Schwann cells and neural stem cells, for NTF expression provides a localized source of trophic molecules as well as a potential growth substrate for axons. Genetically modified Schwann cells have been used to produce and secrete human brain-derived neurotrophic factor (BDNF) and nerve growth factor (NGF). (Menei 1998; Tuszynski 1998) Expression of NGF has been shown to induce growth of primary sensory axons and noradrenergic axons. The delivery of BDNF and neurotrophic factor-4/5 (NF-4/5) in midthoracic dorsal hemisection lesions has been shown to increase growth of primary sensory, noradrenergic coeruleospinal and motor axons. (Blesch 2002)

Similar studies have shown promise in the chemical neutralization of growth inhibitors towards competent axonal growth. (Bregman 1995) Isolation of the myelin-related inhibitor, Nogo, has led to the production of antibodies that bind to and restrain the neuronal growth inhibitor, including inhibitor-neutralizing antibody IN-1. (Schwab 1990; Bregman 1995; Wickelgren 2002) Any pharmacological intervention to SCI must incorporate such inhibitory antibodies with growth factors to promote high degrees of axonal growth and neural regeneration.

Relative success in spinal cord regeneration following cord transection has been elicited when the above factors are incorporated within a controlled environment. The use of semi-permeable, resorbable polymeric conduits has shown significant benefits to axonal regeneration and functionality. (Pinzon 2001; Spilker 2001) Collagen based scaffolds provide support for growing axons as well as reduce the incidence and severity of glial scarring. Furthermore, the cover afforded by the ensheathed environment protects the delicate neural tissue from immunological responses while promoting the formation of tissue cables connecting rostral and caudal spinal cord stumps. Tubes may be seeded with necessary growth factors or genetically modified cells to further improve the biochemical environment. Migration of astrocytes from both rostral and caudal stumps has also been shown to occur

within the lumen environment and may explain the prevalence of regenerated axons with myelin coating. (Spilker 2001) Further studies have shown that the incorporation of other exogenous cells, e.g. Schwann, olfactory-ensheathing glial and neural stem (NS) cells, in coordination with growth factors or vectors of NTF lead to more extensive regeneration. (McDonald 1999)

### **1.6 Objectives of the Current Research**

This study hopes to address the efficacy of entubulated environments in promoting spinal cord regeneration. The use of collagen implants in tissue engineering is driven by its biocompatibility, resorption characteristics and analogous nature to the basal lamina. The ease of manufacturing collagen implants, coupled with its wide availability and low cost, further merit its use.

Collagen implants should serve the wound site as a physical barrier, protecting against the infiltration of exogenous tissues and cells that promote scar formation. Two distinct styles of implant will be evaluated in the transected rat spinal cord; (1) a preformed tubular implant which will lay in the empty vertebral space and (2) a thin bi-layered sheet of collagen which will be wrapped around the lesion. Regenerative capacity will be defined by comparative analysis of tissue morphology, histology and immunohistochemistry.

## **1.7 Relevance of Current Study to the field of Aeronautics and Astronautics**

During a March 2000 hearing before the US House of Representatives Subcommittee on Space and Aeronautics, Dr. Arnauld Nicogossian, then Associate Administrator of NASA's Office of Life and Microgravity Sciences and Applications, testified that

*“The modifications in motor control that occur in microgravity have much in common with those that occur in spinal cord injury, NASA is co-funding research with the National Institutes of Health to address this issue. In a parallel to the microgravity environment, the normal functions of standing and stepping are lost, either wholly or partially, when the spinal cord is injured. Insights gained through understanding these processes also have enormous potential to help people with spinal cord injuries regain at least some use of their legs.*

Research at UCLA continues to offer intriguing evidence that the spinal cord can be taught to relearn walking or standing after spinal cord injury. This research is based upon observations from space flight as well as ground-based research. A clinical trial in which people with spinal cord injuries will be trained to walk on a treadmill is now under way at five centers in the United States using a technology resulting from this NASA and NIH funded research.” (Nicogossian 2000)

Dr. Nicogossian's statement underlies the basis of the current research towards improving the understanding of basic physiological healing and the effects of foreign body implant towards functional regeneration of the spinal cord. A sound understanding of the fundamentals of spinal cord injury rehabilitation necessitates a broad investigation into its pathophysiology. It is hoped that, by understanding the underlying mechanisms of spinal cord regeneration, improvements to rehabilitation may become available to those suffering from spinal cord injuries and various decrements of motor function.

## **Chapter 2: Materials**

### **2.1 Rationale for current material selection**

The rehabilitative use of collagen-glycosaminoglycan (GAG) scaffolds has been utilized for a variety of *in vivo* regenerative processes. Regeneration of guinea pig and human dermis, canine meniscus, as well as rat peripheral and central nerves have been facilitated by the use of collagen-GAG (CG) matrices. (Burke 1981; Yannas 1981; Yannas 1987; Heimbach 1988; Stone 1990; Spilker 1997)

Recent findings linking chondroitin 6-sulfate, a GAG copolymer commonly used in scaffolds of the previously noted research, as an inhibitory species in nerve regeneration have led our group to investigate the efficacy of unmodified collagen scaffolds towards spinal cord regeneration. Work by Harley et al. has already shown the promise of such collagen entubulation in promoting peripheral nerve regeneration. (Harley 2004) The current research will compare the regenerative capacity of collagen (5% w/w) tubes and commercially available collagen sheets.

Another element of the current research is to determine the efficacy of a dorsal barrier to isolate the wound site from adjacent, mainly muscular, tissue. The infiltration of myofibroblasts and the resultant formation of dense fibrous scar tissue in spinal cord injuries impede competent axonal regeneration. (Kiernan 1979; Krikorian 1981; Guth 1985) Previous work in this lab demonstrated the efficacy of CG membranes in dramatically reducing myofibroblast infiltration which was shown to increase the number of axons regenerated across the gap. (Spilker 1997) The current research will hope to show similar results through the use of a collagen dorsal barrier.

### **2.2 Materials Preparation**

#### **2.2.1 Type I collagen tube**

Type I microfibrillar collagen, derived from bovine tendon (Integra Lifesciences, Plainsboro, NJ, USA) was prepared into a slurry suspension (5% w/w) and mixed with a 0.5 M acetic acid solution. Low speed centrifugation of the collagen slurry allowed for the migration of trapped air bubbles, introduced during the mixture process, out of the suspension. The complete protocol for preparation of the collagen suspension is provided in



Appendix A. Collagen tubes were fashioned in injection molds and conferred rigidity and porosity via freeze-drying. The mold was fashioned from two identical Teflon blocks which when secured together provided a single block with six holes (3.3 mm in diameter) drilled lengthwise through the block. The holes were equally spaced and aligned along the center of the assembled block. Images of the mold are provided in Appendix B. To reduce joint stress and possible warping of the Teflon mold, an aluminum shell was secured to each half of the mold. The aluminum provided structural rigidity and maintained tube geometry when the two halves were tightly fastened. Collagen was injected into the assembled mold followed by Teflon coated quartz rods (3.0 mm in diameter) which produced the lumen of the tube geometry.

The mold, containing the tube shaped slurry, was placed in a freeze-dryer (VirTis, Gardiner, NY, USA) and frozen at -40°C for one hour. A vacuum was introduced and the temperature of the freezer environment was gradually increased to 0°C to promote sublimation of ice frozen within the collagen suspension. The resulting porous collagen tubes had an inner diameter of 3.0 mm and an approximate wall thickness of 150µm. Increased cross-linking density, as well as implant sterilization, was afforded to the tubes by holding them at 120°C (vacuum) for 24 h in a Fisher Isotemp 201 Vacuum Oven (Fisher Scientific, Boston, Mass, USA). (Chamberlain 1998) This dehydrothermal environment has been shown to decrease the *in vivo* degradation rate of the collagen implant via covalent linkages between polypeptide chains of the collagen fibers without denaturing the implant. (Yannas 1967)

Cross-linked collagen tubes were removed from sterile packages during animal surgery, as described later, in an aseptic environment. Tubes were cut to a length of 8mm, allowing for sufficient entubulation of caudal and rostral cord stumps at each end of the tube as well as the 5mm gap to be bridged. Prior to implantation, the tubes were hydrated in a sterile saline solution bath. Providing for improved surgical handling, the saline solution also provided an aqueous filling for the implant's lumen.

### **2.2.2 BioGide® collagen membrane**

The BioGide® membrane (Geistlich Pharma AG, Wolhusen, Switzerland) is composed of Types I and III porcine collagen. Its bilayer structure is composed of a smooth surfaced, cell occlusive, compact layer and a second porous layer of loosely organized

collagen fibers. The former is purported to protect against connective tissue infiltration while the latter, porous layer, promotes integration with host tissue through cell invasion and stabilization of the blood clot.(BioGide 2004)

Sterile BioGide® membranes (30x40mm) were individually prepackaged in double blister packs. These commercially available sheets were utilized as two distinct implantation entities for the current research. In aseptic surgical surroundings, the BioGide® membrane was removed from its package and trimmed into strips of either 10x12mm or 8x12mm. The 8x12mm membrane strip was used on certain animal groups as a dorsal barrier and placed over the wound site to obstruct potential myofibroblast infiltration from overlying musculature. The 10x12mm strips were used to entubulate the transection gap like a bandage wrap. The collagen wrap, once fashioned *in vivo* around the transected cord, possessed similar measurements to the preformed collagen tubes, described previously. The wrap bridged the 5mm gap and extended a further 1-2mm to envelop each of the caudal and rostral cord stumps.

Unused portions of the BioGide® membrane were sealed in sterile containers and used for subsequent surgeries.

### **2.3 Material Characteristics**

Two properties of the collagen entubulation implants – pore volume fraction (porosity) and average diameter – have previously been defined as contributing to the regenerative capacity of extracellular matrix analogs. (Yannas 1989; Chamberlain 1998)

Sections of the collagen tube and the BioGide® wrap were embedded in JB-4 Resin (Polysciences, Warrington, PA). For the sake of analytical conformity the BioGide® membrane was rolled into a tubular shape during the solidification of the resin. Positioned such that its porous layer created the tube's lumen, this orientation approximated the geometry of the implanted wrap *in vivo*. Samples were sectioned transversely and longitudinally at 5µm with a microtome, mounted onto standard slides, stained with aniline blue and then coverslipped. Aniline blue enhanced pore analysis by providing a contrast of collagen against neighboring pores. Images of the sections were taken at low magnification (10x) with a light microscope outfitted with a digital camera (Olympus BX51TF, Olympus Optical Co., Japan) interfaced with a personal computer (eMac, Apple, USA). Sample images

of the stained samples are provided as Figures 2.1 and 2.2. These cross-sectional images were taken at 1.25x magnification to provide the reader a wider viewing aspect of each implant than afforded by stronger magnifications. Digitized images were opened in Adobe Photoshop (Adobe, San Jose, CA) and individual pores were outlined in black to create explicit contrast between pore and collagen. These images were then analyzed using ImageJ software (available as freeware from NIH, Bethesda, MD) to count the total number of pores and provide their respective area and perimeter measurements. Porosity was defined as the fraction of overall pore area to total scaffold area (which included pores and collagenous material) while pore diameter was defined by the pore's hydraulic diameter. A true circular pore diameter was difficult to generate because sections may have been cut at odd or tangential angles to pore orientation; the hydraulic diameter was used to normalize these variations. Hydraulic diameter is defined as

$$D_h = (4 * A_{\text{pore}}) / P_{\text{pore}}$$

where  $D_h$  is the hydraulic diameter and  $A_{\text{pore}}$  and  $P_{\text{pore}}$  are the implant pore area and perimeter, respectively.

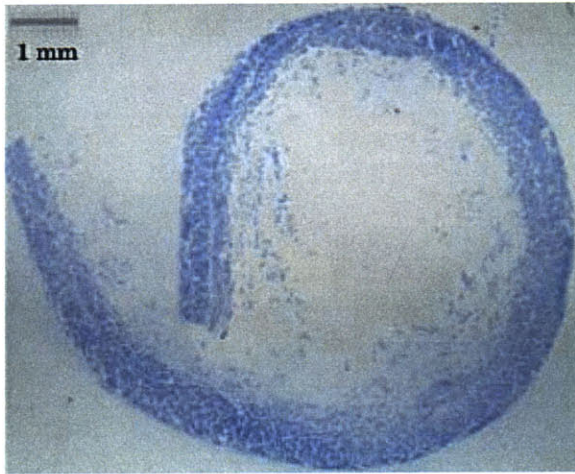


**Figure 2.1** – Cross-sectional image at low magnification (1.25x) of the BioGide® membrane wrap into a tubular shape. The implant was embedded in JB-4, sectioned at 5µm thickness and stained in Aniline Blue.

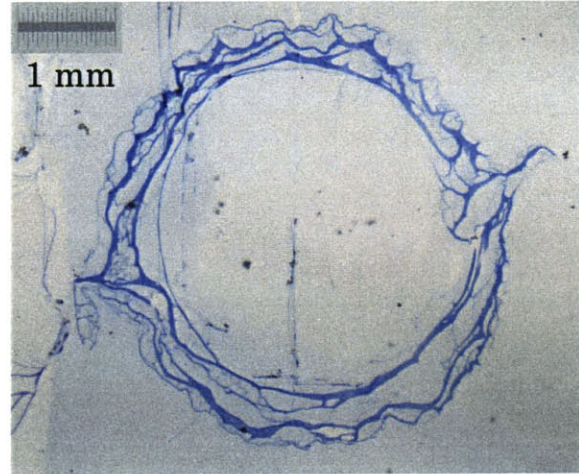


**Figure 2.2** – Cross-sectional image at low magnification (1.25x) of a Type I bovine collagen (5% w/w) tube. The implant was embedded in JB-4, sectioned at 5µm thickness and stained in Aniline Blue.

## 2.4 Results

### 2.4.1 Average Pore Diameter

The results from the ImageJ analysis of pore geometry, i.e. perimeter and area, were used to derive the hydraulic pore diameter for both the collagen tube and BioGide® membrane. The results were averaged over the many sample sections and have been listed in Table 2A along with respective standard deviations.

**Table 2A** – Measured hydraulic pore diameters of collagen implants.

	Average Hydraulic Diameter ( $\mu\text{m}$ )
Collagen tube	37.80 +/- 53.88
BioGide® membrane	8.01 +/- 3.91

### 2.4.2 Average Porosity

The results from the ImageJ analysis of total pore area was normalized with respect to total scaffold area to provide a quantitative value of porosity. An average porosity was taken over the many images analyzed for both implants and can be found in Table 2B.

**Table 2B** – Measured porosities of collagen implants.

	Average Porosity (percent)
Collagen tube	66.7 +/- 6.5
BioGide® membrane	51.1 +/- 4.2

These results show a noticeably larger porosity (67%) for the tubes manufactured in our lab than the commercially available BioGide® membrane (51%). Similarly, the tubes contained much larger pores (average of  $38\mu\text{m}$  in diameter) than those of the BioGide® membrane ( $8\mu\text{m}$ ). Moreover, Table 1 shows a wide variation amongst pore diameters of the tube and suggests a relatively high degree of pore geometry heterogeneity. These quantitative

results may be qualitatively confirmed by visual inspection of Figure 2.2. Large macroscopic pores, randomly interspersed amongst densely packed small pores, are evident in large numbers all along the tube walls. This is in contrast to the BioGide® membrane which exhibits fairly consistent pore characteristics. Figure 2.1 further illustrates the relative uniformity of pore size and distribution throughout the membrane.

Another striking characteristic apparent from inspection of Figures 2.1 and 2.2 is the relative density of collagenous material of each implant. The staining of the BioGide® membrane exhibits a continuity of hue and color saturation within each of its two distinct collagenous regions, the compact layer staining darker than the porous layer. The density of the stained color is much greater, however, within the collagen struts of the tube's walls. Since all samples were stained concurrently, in accordance with accepted staining protocols, it may be assumed that the tube's manufacture process causes the aqueous collagen suspension to preferentially organize itself into dense tracts of collagen fibers. These differences in color density, which allude to a difference in collagen fiber density, may lead to discernable disparities in the *in vivo* degradation of each implant.

## 2.5 Discussion

A few remarks about the microscopic characteristics of the implants are necessary. Determining an average hydraulic pore diameter for the BioGide® membrane is slightly more obfuscated than represented, especially with respect to the layer facing the lumen. Portions of the porous layer, composed of loosely organized collagen fibers, were difficult to include in the overall pore analysis. The lumen of the BioGide® wrap implant in Figure 2.1 contains many bits and disjointed strands of collagen; its overtly loose composition made explicit demarcations of pore structure impossible. Highlighting the accepted limitations in analyzing cross-sectioned samples, there was no suitable method to extrapolate an accurate geometric representation of these inner pores. The results listed in Table 2A were deemed acceptable since the unanalyzed portion of the wrap implant composed only a small fraction of the overall implant cross-sectional area. All the pores of the thicker, outer layer, as well as a majority of the pores within the inner layer, excluding those described above, were accounted.

Table 2A shows a greater degree of control in pore size characteristics within the BioGide® membrane than the collagen tube. The notable variation in pore sizes of the tube

was an unexpected effect of modifications to manufacturing protocol established in this lab. The original protocol was designed for production of thick walled (750 $\mu$ m), small diameter (1.5mm) tubes for use in peripheral nerve regeneration. (Spilker 2000) The constraints of size and space within the rat spinal cord environment necessitated changes in tube geometry to an inner diameter of 3.0mm with a wall thickness of 150 $\mu$ m. These modifications in tube design, especially the dramatically reduced wall thickness, may result in decrements to shear strength and buckling capacity.

The original protocol required that the collagen suspension, following an initial *in situ* freezing at -40°C, be removed from its mold and mandrels prior to vacuum-induced sublimation. This had allowed for an uninhibited escape of ice crystals from the collagen and resulted in fairly controllable pore creation. Attempts to remove the larger, thin walled, tubes from the mold and individual mandrels resulted in destructive shearing. To avoid compromising tube integrity, the entire manufacture process was conducted with the aqueous collagen slurry kept in its mold and mandrels left in place. The modified protocol is provided in Appendix A. Ice crystals were still able to sublime from the tubes and escape through the mold. However, the evacuation of ice crystals was nowhere as unrestrained as when the tubes had been directly exposed to the vacuum, as provided for in the original protocol.

Changes to the manufacturing protocol may also be responsible for creating highly dense tracts of collagen along the inner and outer faces of the tube's wall. Previous work in this lab with collagen and collagen-GAG matrices has shown that a non-porous collagen skin forms along surfaces where the suspension is in contact with its container. The modified manufacturing protocol left the collagen suspension within its mold and resulted in the formation of a dense outer skin. The dense inner skin was an artifact of the suspension's contact with the mandrel. The existence of these dense skins can be seen in Figure 2.2 as the two richly stained concentric bands.

Dense collagen formation within the tubular scaffold may induce slower *in vivo* degradation rates than those of the BioGide® membrane. Such discernable differences between implant resorption kinetics may affect axonal regeneration. However, other structural factors play significant roles during the resorption process; the greater thickness and flexural strength (qualitatively based on manual handling) of the BioGide® membrane may compensate for collagen density and balance relative *in vivo* degradation rates. Since the

current research deals more with the feasibility of implants in promoting central nerve regeneration, a thorough investigation in degradation rates was deemed unnecessary. Any future work, should it be warranted, would require an attempt to optimize axonal regeneration through modifications in implant design and characteristics.

## **Chapter 3: Methods**

### **3.1 Injury Model**

Various models have been designed to reproduce the functional deficits resulting from traumatic spinal cord injury. Crushing trauma to the spinal cord has been reproduced surgically with forceps. (Guth, Barrett et al. 1985; Midha, Fehlings et al. 1987; Theriault and Tator 1994) Contusion, or blunt trauma, injuries have been modeled by groups dropping a weighted piston directly onto the naked cord. (Blight and Decrescito 1986; Stokes and Reier 1991; Basso, Beattie et al. 1996; Beattie, Bresnahan et al. 1997) Although such techniques accurately model the trauma evident in clinical spinal cord trauma, their use for the study of central nerve regeneration has limitations. Such models might not provide reproducible deficits to distal limb function and therefore prove unreliable in assessing rehabilitation, qualitatively or quantitatively. Compression or contusion injuries may not result in complete paraplegia; certain portions of the spinal cord may remain unaffected leading to collateral sprouting of those undamaged central axons. Such functional recovery might lead to incorrect assumptions about regeneration success.

Other surgically induced trauma models have been devised to mimic spinal cord injury. Hemisection and transection models utilize surgical incisions half-way through and completely through the spinal cord, respectively. (Liu 1981) The model utilized in the current research is a transection of the spinal cord at T7 and T9, including complete detachment of intermediary ventral and dorsal roots. A gap is formed by removing the ~5mm section of cord between these incision points; this gap transection may also be referred to later as simply gap or transection.

### **3.2 Animal Model**

The most widely accepted animal model for investigative research on spinal cord regeneration is the adult rat. Although other models have been successfully attempted, such as feline, canine and primate, the rat model has provided repeatable results with sufficiently low mortality rates.

Following a gap transection of the spinal cord the adult rat loses motor and sensory function distal to the insult. A gap transection at T7-T9 results in loss of lower limb function



including the temporary loss of reflex bladder control. Certain anatomical features of the female rat promote its use over the male rat. The ease in finding the former's bladder and shorter urethra facilitate manual expression of urine from the bladder. The current research utilized adult (12 week old) female Sprague Dawley rats (Taconic, Germantown, NY).

All surgical procedures, pre and post-operative care, were performed at the Animal Research Facility (ARF) of the Veterans Administration Medical Center (Jamaica Plain, MA) with diligence paid to following federal guidelines regarding laboratory animal care. (Institute of Laboratory Animal Resources 1996) Surgery was conducted under aseptic conditions in the main surgery room of the ARF. Rats, weighing 250-350 grams, were anesthetized by an intraperitoneal injection of either sodium pentobarbital (Nembutal solution, 50 mg/ml, Abbott Laboratories, North Chicago, IL) with a dosage of 45 mg/kg or a ketamine/xylazine cocktail (Ketaset, 100 mg/ml, Fort Dodge Animal Health, Fort Dodge, IA; AnaSed, 20 mg/ml, Lloyd Laboratories, Shenandoah, IA) with a dosage of 0.2 ml/250 kg and 0.1 ml/250 kg, respectively. A constant flow of oxygen was delivered to the animal during surgery via a nose cone. Anesthetized animals were prepped for surgery with shaved backs and the use of a povidone iodine disinfectant scrub (ScrubCare, Allegiance Healthcare Corp., McGraw Park, IL). The animal was set prone on a flat operating board with limbs gently constrained in an extended position with rubber bands.

The surgical procedure was similar to that of a previous study within our group. (Spilker 1997) A 2 inch longitudinal incision was made along the back, running between the shoulder blades to just below the rib cage. Underlying musculature was incised and retracted laterally exposing the dorsal aspect of the thoracic vertebrae. A laminectomy of segments T6-T11 was performed, with bone rongeurs and fine surgical scissors, exposing approximately 10 – 15mm of thoracic spinal cord. Minor bleeding was controlled with Gelfoam (The Upjohn Co., Kalamazoo, MI) and local anesthesia (Lidocaine, 20 mg/ml, Biomed Inc., Riverside, MO) was provided as necessary upon the open wound.

The dura mater was incised at the midline using a #11 blade. The blade was then run transversely along the vertebral body at sections T7 and T9. Removal of the intermediary cord, facilitated by use of surgical scissors to excise peripheral roots, left a 5-mm gap. Gelfoam was temporarily placed in the gap to promote hemostasis.

Five experimental groups were established in accordance to the type of implant inserted into the gap. Group I, the control group, received no implant to artificially bridge the excised gap. Group II was similar to the control group except for the incorporation of a collagen dorsal barrier. These groups were designed to observe the native regenerative ability of the spinal cord. All dorsal barriers, cut from the BioGide® membrane, were draped over the lesions and extended 2-3mm past

the rostral and caudal stumps to separate the transected gap from overlaying musculature. Groups III and IV were implanted with collagen (5% w/w) tubes with Group IV also receiving a dorsal barrier. The tubes were trimmed as necessary to allow the rostral and caudal stumps of the cord to rest 1-2mm inside each end of the tube. The final experimental group,

Group V, was implanted with a strip of BioGide® membrane. The strip was positioned inside the vertebral cavity and gently positioned on the surface of the vertebral body and then folded over to create a bandage-like wrap around the transected gap. The strip was trimmed such that 1-2mm of each cord stump would be wrapped within its lumen. A dorsal barrier was then draped over the wrap implant. The groups are illustrated together in Figure 3.1 and listed in Table 3A.

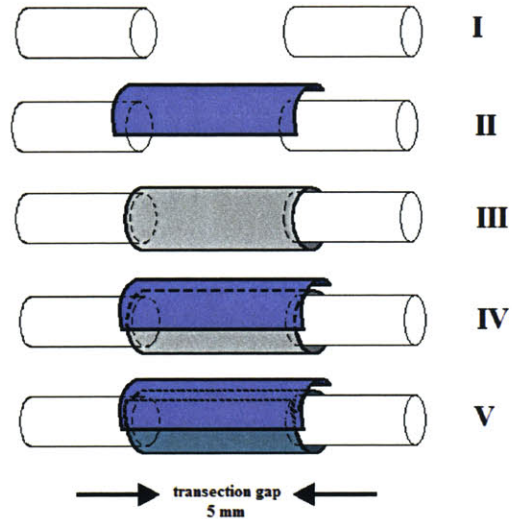


**Figure 3.1** – An illustration (not to scale) of the five different experimental groups and their respective implants.

**Table 3A** – Experimental Groups

Group	Implant Received
I	None (Control)
II	Dorsal barrier
III	Collagen (5% w/w) tube
IV	Tube w/ dorsal barrier
V	Collagen wrap w/ dorsal barrier

All collagen implants had been soaked in a sterile saline solution for approximately ten minutes prior to implantation. The soaking provided improved pliability and ease of placement within the vertebral environment. Each tubular implant was carefully filled with the sterile saline to ensure that no air bubbles remained. Images of the tube implantation can be seen in Figures 3.2 - 3.6; images of the wrap and dorsal barrier implantation can be seen in Figures 3.7 - 3.9.

Retracted muscles were then closed in layers using 4-0 vicryl sutures (Johnson and Johnson, Sommerville, NJ) and skin was secured with wound clips. Animals were given 1 ml of Lactated Ringers Solution (LRS) subcutaneously (SC) immediately post surgery to replenish fluid and electrolytes lost during surgery. Animals were placed on heating pads with supplementary heat provided by the intermittent use of heat lamps to maintain an adequate body temperature (as measured via rectal thermometer). Depending on the type of anesthesia, animals remained unconscious for 2 to 6 hours (with animals receiving Nembutal remaining unconscious longer than those receiving the ketamine/xylazine combination).

Upon returning to consciousness, animals were placed in plastic cages with wood chip bedding, food and water. Animals received another 2 ml of LRS injected SC and started on a regimen of analgesics and antibiotics. SC injections of 0.15 ml Cefazolin (100 mg/ml) and intramuscular injections of 0.1 ml buprunorphine (Buprenex 0.3 mg/ml) were administered daily for the first week post-op. Animals were then given a quarter tablet of cephalexin (Keflex, 250 mg) daily for the second week post-op to ingest at their own volition. Medication was not administered following the second post-operative week although readministration of cefazolin was contingent upon signs of bladder infection. Animals were housed and intermittently groomed in Room 202 of the ARF.

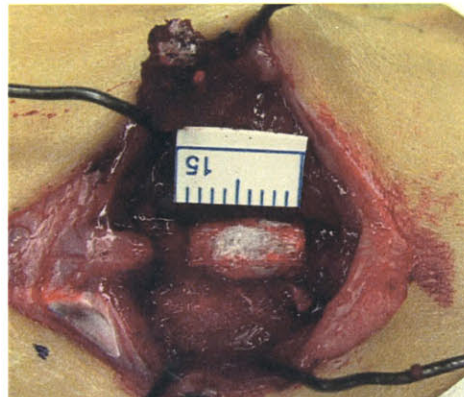
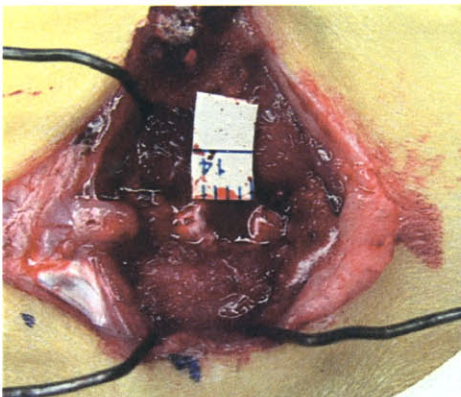
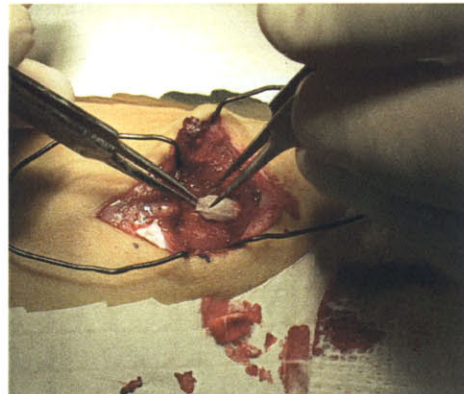
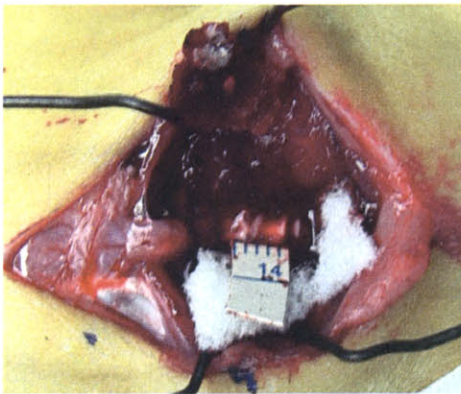
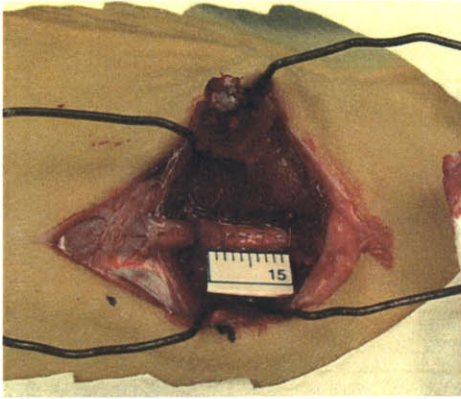
**Figure 3.2 (top left)** – Following laminectomy, 10-15 mm of intact spinal cord was exposed.

**Figure 3.3 (middle left)** – Complete transections were made across the seventh and ninth thoracic segments (T7 and T9) of the exposed spinal cord.

**Figure 3.4 (bottom left)** – The portion of cord between T7 and T9 was removed leaving a 5 mm gap transection.

**Figure 3.5 (top right)** – The collagen tube, having been soaked in a sterile saline bath, was implanted into the lesion site. Shown here, the caudal stump is being placed within the lumen of the tube.

**Figure 3.6 (bottom right)** – Implantation of the collagen tube, Group III, was followed by suturing together retracted muscle and closing the wound. A collagen membrane (or dorsal barrier) was draped over the tube for Group IV animals.



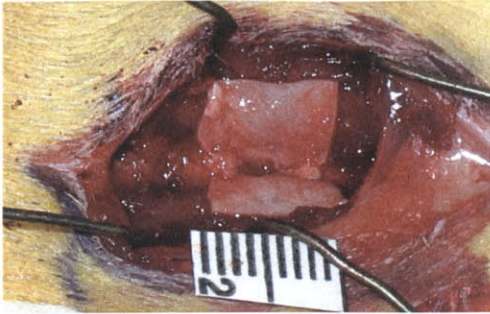
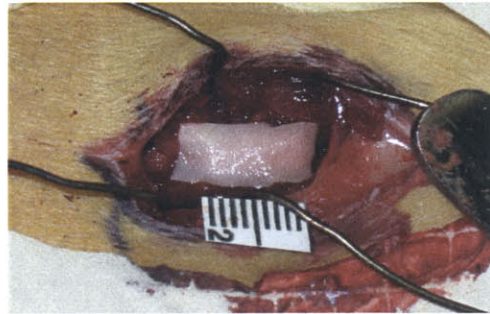
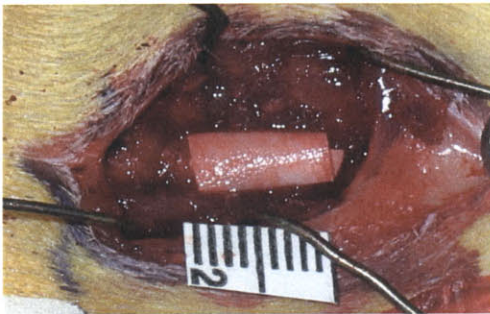


**Figure 3.7 (top left)** – A collagen sheet, approx. 10 x 12 mm, was slid beneath the spinal cord stumps.

**Figure 3.8 (bottom left)** – The ends of the sheet were folded over to completely enwrap the lesion site.

**Figure 3.9 (bottom right)** – A dorsal barrier, approx. 8 x 12 mm, was draped over the collagen wrap before overlying muscle was sutured together and the wound closed.



### 3.3 Animal Sacrifice

Rats were sacrificed via carbon dioxide inhalation four weeks (28 days) post-operatively. Caged animals were individually transferred into a sealable plastic container. The container was fitted with an inlet nozzle connected to a tank of CO<sub>2</sub>. CO<sub>2</sub> gas was allowed to run through the container for up to 5 minutes to ensure complete and proper euthanization.

### 3.4 Tissue Retrieval and Processing

Euthanized rats were taken to the main operating room of the ARF where skin and musculature above the spinal column were incised. The entire thoracic spinal cord (about 20mm in length) including the lesion site was removed with scalpel and blunt-nose surgical scissors and stored in 10% neutral buffered formalin at 4°C for 48 hours. Overlying musculature was then carefully removed from the surface of the transverse process and vertebral body, only some soft tissue was removed from the vertebral laminar area for fear of damaging the underlying, covered implant. The gross specimen was stored in a fresh formalin bath at 4°C for another 24-48 hours to permit sufficient infiltration into the spinal cord and promote specimen dexterity during manipulation and handling. Bone ronguers and fine

surgical scissors were used to gently remove the remaining vertebrae from the cord. The lesion site was easily identified on the naked cord because of its slight discoloration and



**Figure 3.10** – An image of the explanted spinal cord from an animal in Group V, receiving a wrap and dorsal barrier. The implant appears slightly off color from the normal cord tissue; overlying soft tissue can be seen to have fused to the surface of the implant.

reduced cross sectional area. In all cases, the overlying soft tissue had fused to the surface of the implant (or dorsal barrier) and was left on the excised cord sample so as not to risk damaging the reparative tissue. Figure 3.10 shows the explanted tissue from an animal of Group V.

The center of the gap defect was estimated based on visual inspection and a number #11 blade was used to cut the cord into two segments. Measuring from the center of the defect, 5mm sections were taken caudally and rostrally from the center of the defect and labeled C and R, respectively. The rostral portion would be used for further analysis of axonal regeneration while the caudal segment would be used for conventional histology and immunohistochemical analysis. Remaining portions of the spinal cord were stored in formalin should their use be deemed necessary.

### **3.4.1 Rostral Segment**

The 5mm spinal cord segment rostral to the center of the defect was used to define the relative degree of axon regeneration permitted through the gap. The sample was post-fixed in 1% osmium tetroxide (to stain for myelinated axons), dehydrated through graded alcohols and then embedded in epon (PolyBed 812, Polysciences Inc., Warrington, PA). Transverse cross-sections were cut at 1.5 $\mu$ m on an ultramicrotome (MT-X Ultramicrotome, RMC, Tucson, AZ) and captured on glass microscope slides. Sections were stained with 1% toluidine blue solution and then coverslipped.

Stained sections were then examined at 100x by a light microscope outfitted with a digital camera. The entire tissue sample was examined in an orderly fashion such that every distinguishable myelinated axon was digitally captured and stored on a personal computer interfaced with a microscope.

### ***3.4.2 Caudal Segment***

The 5mm spinal cord segment caudal to the center of the defect was used for histological and immunohistochemical analyses of the tissue regenerated within the gap. Samples were placed in individually labeled tissue processing cassettes and processed for, then embedded in paraffin (HypercenterXP Tissue Processor, ThermoShandon, Houston, TX). Transverse cross-sections were cut at 7 $\mu$ m with a microtome and captured on glass microscope slides.

Histological evaluation would be performed by separately staining the samples with hematoxylin and eosin (H&E) for general cell identification and Masson's trichrome to identify the presence of collagenous tissue. Captured samples were deparaffinized, hydrated, stained and then coverslipped. Images of the sections were taken at 40x magnification and an identification and gross count of various cells were made to express degree of inflammation, scaffold resorption, collagen formation and possible anomalous responses within the lesion site.

Immunohistochemical evaluation of each sample was based on astrocyte proliferation, degree of axonal regeneration and smooth muscle infiltration. Astrocyte proliferation was identified by polyclonal rabbit anti-glial fibrillary acidic protein primary antibody (anti-GFAP; Zymed Laboratories Inc., San Francisco, CA), diluted 1:6; axon regeneration was expressed by monoclonal mouse anti-68 kDa neurofilament antibody (EnCor Biotechnology, Inc., Alachua, FL), diluted 1:400; smooth muscle infiltration was expressed by anti- $\alpha$  smooth muscle actin (anti-SMA) antibody (Sigma-Aldrich, St.Louis, MO), diluted 1:400. Samples were deparaffinized, hydrated and then placing into an autostainer (Dako Autostainer Plus; Carpinteria, CA) where slides were incubated with the primary antibody, anti-GFAP diluted 1:6 and anti-68kDa diluted 1:400, for 15 minutes at room temperature. Samples were then rinsed three times for five minutes each in PBS and then incubated for 20 minutes in an appropriate biotinylated secondary antibody solution. Duplicate samples were similarly processed except for replacement of each primary antibody with nonimmune serum as controls to verify antibody specificity. Sections with anti-GFAP primary antibody were incubated in biotinylated goat anti-rabbit IgG diluted 1:400; sections with neurofilament primary antibody and anti-SMA were incubated in biotinylated goat anti-mouse IgG diluted 1:400. Slides were reacted with avidin-biotin complex and developed with a

diaminobenzidine (DAB) chromogen solution (for the anti-GFAP and anti-68 kDA samples)  
or 3-amino,9-ethyl-carbazole (AEC) solution (for the anti-SMA samples).



## Chapter 4: Results

### 4.1 General Observations

The animals of the study experienced a survival rate of 83%, with 19 of 23 rats surviving post-surgery. The number of animals in each group, as well as the implant each group received, is listed in Table 4A. One rat exhibited autotomy five days prior to sacrifice and was given 0.10 ml of bupronorphine daily. All animals lost hindlimb function distal to the

**Table 4A** – Experimental groups and the number of rats within each.

Group	Implant Received	Number of Rats
I	None (Control)	3
II	Dorsal barrier	4
III	Collagen (5% w/w) tube	4
IV	Tube w/ dorsal barrier	4
V	Collagen wrap w/ dorsal barrier	4

insult but maintained adequate forelimb mobility, grooming and consumption of food and water (provided ad libidum). As described previously, temporary loss of the reflex bladder voiding function required manual expression of the bladders three times daily, or as deemed necessary, until function was

restored - usually within two weeks. No formal assessment of hindlimb motor function recovery was made, however, no animal regained the functional or weight bearing capacity of the hindlimbs.

### 4.2 Morphological Observations

The excised spinal cord tissue of every animal group, including Groups I and II, revealed a cord of reparative tissue that bridged the gap between rostral and caudal cord stumps. Low magnification (1.25x) images of the epon embedded cross-sections were analyzed with ImageJ software. The cross-sectional area of the regenerated tissue was found to range from roughly 1 to 3 mm<sup>2</sup>. Group I exhibited the largest areas while Group III contained the smallest. Table 4B provides the findings, averaged across each group, of the cross-sectional area. Because few regenerated cord samples exhibited pure circular conformation, measurements of the major and minor axes and degree of circularity (where 1.0 indicates a pure circle and 0.0 indicates an increasingly elongated polygon) were included in Table 4B.

A gross observation of all implants, Groups II-V, showed some degree of resorption. Low magnification images showed that the tube implants of Groups III and IV exhibited major fractures, breaking into large pieces. The stress of overlying musculature and skin may have produced enough stress to cause the damage; the tube no longer provided a complete entubulation of the regenerated tissue. Just as stress from overlying tissue was thought to have fractured the tube implants, such stresses induced compressive warping of the wrap and resulted in ovular shaped reparative tissue within the implant. Such compression was also noticed within the dorsal barrier of Group II. These qualitative observations are qualified with the circularity values in Table 4A. Figures 4.1 and 4.2 illustrate the effects of *in vivo* loads on cord morphology and the structural integrity of the implants.

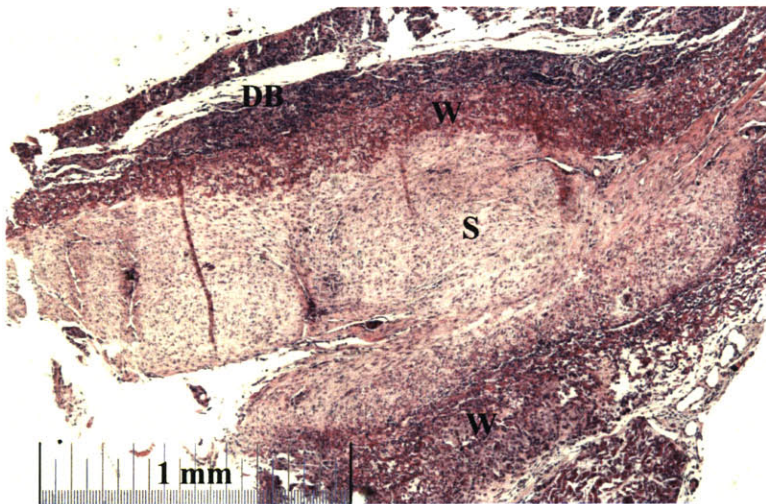


**Figure 4.1** – A low magnification (4x) image of an explant (following 4 weeks *in vivo*) from Group V. The image shows the non-circular morphology of regrown tissue induced by stress from overlying soft tissue and muscle. The image also shows the ingrowth of tissue along the lumen of the wrap. DB-dorsal barrier, W-collagen wrap, S-regrown spinal tissue

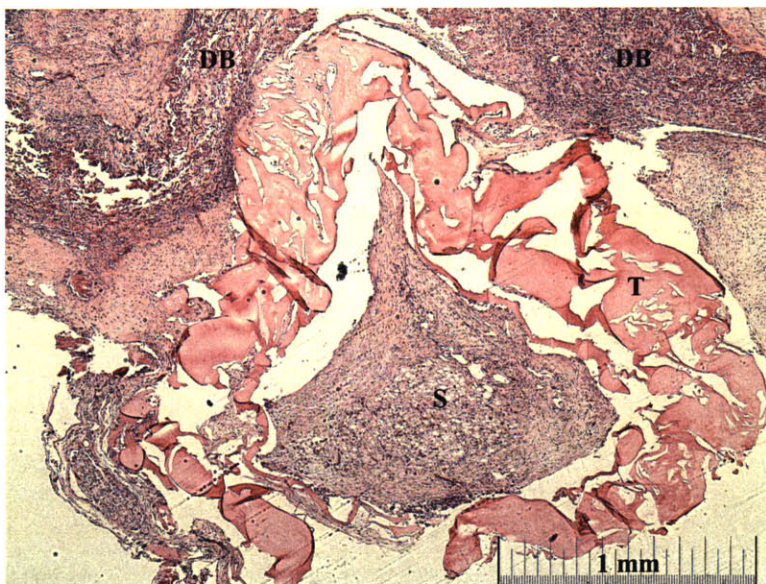


**Figure 4.2** – A low magnification (4x) image of an explant (following 4 weeks *in vivo*) from Group IV. The image shows multiple fractures along the tube induced by stress from overlying soft tissue and muscle. A lack of implant/tissue cohesion is evinced by large gaps between the tissue's surface and the implant's lumen. DB-dorsal barrier, T-collagen tube, S-regrown spinal tissue

**Table 4B** – A summary of the general morphology of regrown spinal cord tissue cross-sections

	Area (mm <sup>2</sup> )	Major Axis (mm)	Minor Axis (mm)	Circularity
Group I	2.96 ± 1.03	2.51 ± 0.43	1.47 ± 0.27	0.67 ± 0.10
Group II	2.59 ± 1.15	2.65 ± 0.34	1.23 ± 0.51	0.55 ± 0.14
Group III	0.69 ± 0.50	1.17 ± 0.35	0.69 ± 0.29	0.56 ± 0.26
Group IV	1.23 ± 0.63	1.69 ± 0.03	0.94 ± 0.49	0.48 ± 0.27
Group V	1.25 ± 0.58	1.53 ± 0.19	1.01 ± 0.38	0.58 ± 0.18

### 4.3 Observations from Histology

Staining with H&E identified the dominant cell types as fibroblasts (laying collagen of varying densities) and macrophages (engulfing debris from necrotic tissue and myelin degradation). The absence of polymorphonuclear neutrophils, lymphocytes, and granulocytes confirmed that the collagen implants did not elicit prolonged inflammatory reactions or foreign body responses four weeks post-implantation.

Low magnification examination of Groups I and II showed competent bridging of the spinal cord stumps. These samples showed fairly active macrophage activity and vascular development. Masson's trichrome (MT) revealed the regenerated tissue to be composed of highly dense, crimped collagen. Crimping of collagen is usually concomitant with the infiltration of myofibroblasts and typical of fibrous scarring. Such an impermissible environment acts as a barrier to the delicate growth cone of the regenerating axon. (Harley 2002) The severity of collagen density and cellular activity was markedly worse in tissue explanted from Group I, without the dorsal barrier, than those within Group II, with the barrier.

As noted before, fracture of the tubes was evident. Collagen tissue within the tube was spotted with areas of dense, crimped collagen and large blood vessels, although at a reduced level than apparent in Group I. The incorporation of the dorsal barrier with the tube, Group IV, elicited fewer indications of fibrous scar formation than with the tube implanted alone (Group III). The interior lumen of the wrap implant (Group V) was found to be extremely

hospitable to axonal regeneration; fibroblast activity and macrophage mediated reorganization of collagen fibers had produced a loose matrix of collagen. Absent from this tissue were the appearance of large blood vessels or fibrous scarring noted in Groups I and III. Figures 4.3 and 4.4 provide a visual comparison of relative collagen densities between Groups II and V.

The exterior, or portions in contact with exogenous soft tissue, of the BioGide® wrap implant, Group V, exhibited much greater macrophage and fibroblast activity than the tube. Large portions of the tube remained intact with little sign of active degradation or resorption. BioGide® derived implants (as found in Groups II, IV, and V) exhibited marked fibroblast and macrophage activity. Histological evaluation, showing signs of active resorption of the membrane, concurred with similar observations from low scale images of thinning (resorbed) regions of both wrap implant and dorsal barrier.

The BioGide® membrane was also found to form coherent bonds with the spinal cord's tissue. The spinal stumps and surface of the regenerated tissue were securely fused to the porous inner layer of the BioGide® membrane. Similar examination found that the tube implants, Groups III and IV, did not achieve any notable degree of cohesion with surrounding cord tissue or the regenerated tissue. Low magnification images showed a continuous empty space between the tube implant and regenerated tissue. Figure 4.1 illustrates the ingrowth of collagenous tissue within the lumen of the wrap and the relative homogeneity of the implant/tissue interface. Figure 4.5 depicts a portion of this interface at a higher magnification. Strands of collagen from the porous membrane layer of the BioGide® wrap are intimately surrounded by native collagen and macrophages. Figure 4.2 shows the contrary for the tube implant, large gaps persist along both interior and exterior faces of the tube. Figure 4.6 provides a higher magnification depiction of the trivial degree of tube implant/tissue cohesion. The tube also exhibits far less engagement with macrophages than the wrap membrane and may be assumed to degrade much more slowly.

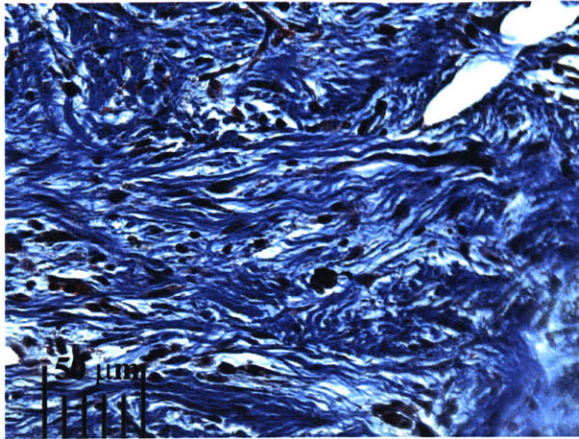


**Figure 4.3** – A higher magnification (40x) image of tissue formed within the transection gap of a Group II explant (following 4 weeks *in vivo*). The tissue is composed of dense collagen, stained dark blue by MT. Crimping of the dense collagen fibers alludes to myofibroblast infiltration and the formation of fibrous scar. Macrophages and fibroblasts appear as dark red spots throughout the image, the former are round while the latter are spindle shaped.

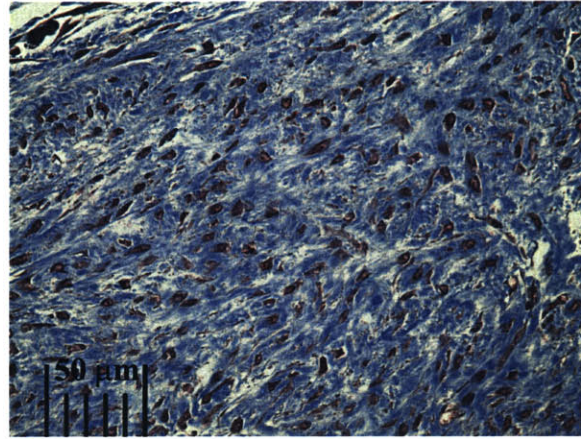


**Figure 4.4** – A higher magnification (40x) image of tissue formed within the wrap implant of a Group V explant (following 4 weeks *in vivo*). The collagen exhibits no preferred orientation and contains a uniform distribution of macrophages and fibroblasts. The collagen appears more globular, without any signs of crimping and may be assumed more permissive to the growth cone of a regenerating axon.

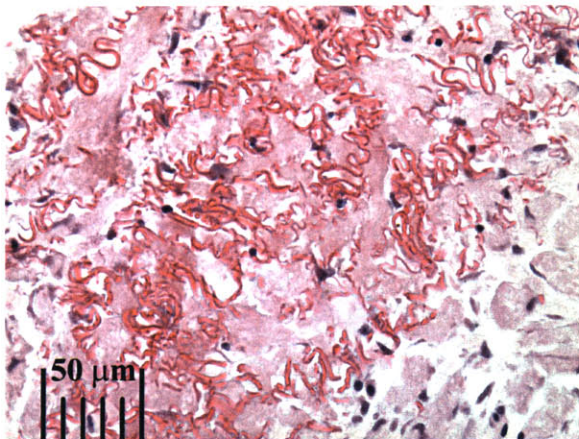


**Figure 4.5** – The lumen of the wrap membrane in Group V has integrated with host tissue. Strands of the BioGide® porous membrane, stained bright pink by H&E, are surrounded by newly laid collagen. A noticeable proliferation of macrophages, responsible for implant degradation and collagen reorganization, are found within this implant/tissue interface.

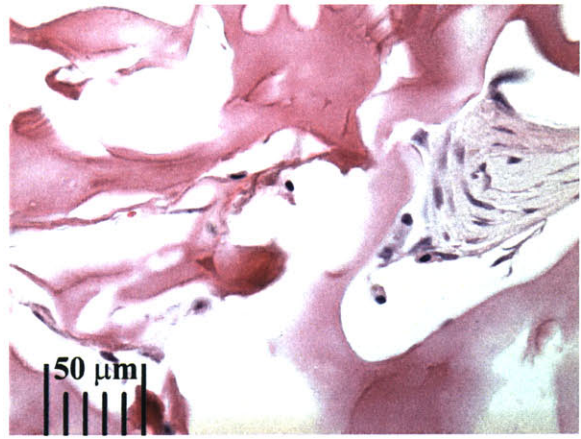


**Figure 4.6** – The lumen of the tube implant in Group III showed very little active integration with newly laid collagen, stained light pink with elongated dark spots (fibroblasts). The tube demonstrated little capacity for promoting cohesive bonds with host tissue. Macrophage activity along and within the walls of the tube was sparse; a coherent implant/tissue interface was equally elusive to find.

#### 4.4 Observations from Immunohistochemistry

The use of collagen based scaffolds has previously been shown effective towards hindering the formation of barriers to competent tissue regeneration. (Harley 2002) For the nervous system, two major species have been well identified towards blocking regeneration –

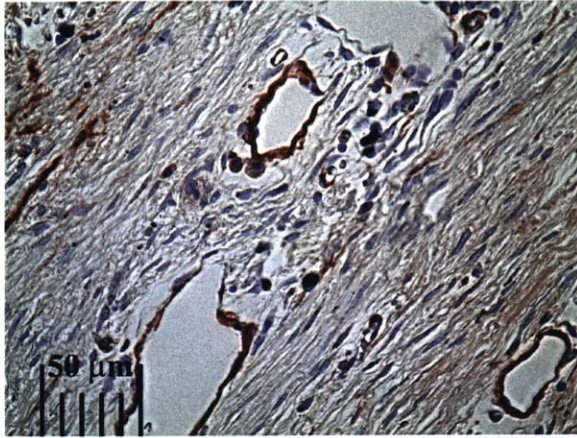


**Figure 4.7** – The infiltration of SMA within the tissue of a Group II explant is shown in red stain. The circular walls of blood vessels stain dark red. The collagenous areas stained with a red hue represent the dense, crimped collagen associated with fibrous scar.

the fibrous scar and the glial scar. Tissue sections were separately stained with antibodies for GFAP and  $\alpha$ -Smooth Muscle Actin (SMA). GFAP is a major component of the glial scar and GFAP antibodies positively stain reactive astrocytes much more strongly than normal astrocytes. The presence of SMA, as expressed by myofibroblasts, has been shown to produce contractile forces in the peripheral nerve wound site. (Harley 2002) The formation of a contractile capsule, or fibrous scar, of connective and contractile tissue forms around the transected stump.

Histological evaluation, as described previously, provided insight into the orientation and organization of connective tissue associated with fibrous scar. Antibodies for SMA stain elements of the contractile tissue and depict the relative severity of fibrous scarring. Light microscopy of the samples at 40x magnification was used to evaluate the presence of these proteins and the relative degree of scar formation.

Similar results were found for both proteins within the experimental groups. Group I and III stained with the highest levels of both scar moieties. The presence of the dorsal barrier (Groups II, IV and V) provided notable protection from scar infiltration. GFAP and SMA expression amongst the groups receiving the dorsal barrier was notably less than Groups I or III. Group II expressed the highest levels of GFAP and Group V the least amongst the groups with a dorsal barrier. SMA expression was minimal and indistinguishable amongst Groups IV and V but significantly higher in Group II.

## 4.5 Axonal Regeneration

Rostral halves of each explant were post-fixed in 1% osmium tetroxide to stain for myelin. Samples, embedded in epon, were sectioned and stained with toluidine blue to

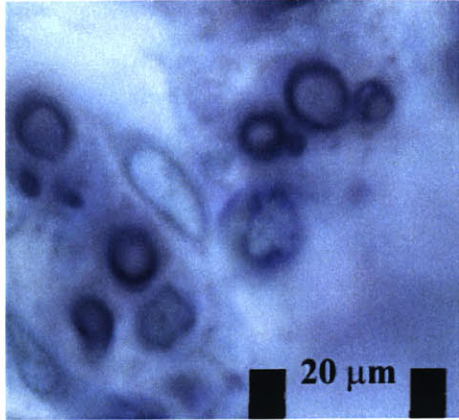


**Figure 4.8** - Regenerated axons were identified by their thick myelin sheaths, stained dark blue. The osmium tetroxide preferentially stains against myelin, allowing visual discrimination of axons from neuroglia and other native cells.

provide greater contrast among cellular elements. Light microscopy of the 1.5  $\mu\text{m}$  sample cross-sections at 100x magnification were used to assess axon regeneration through the center of the lesion. Regenerated axons, as seen in Figure 4.8, could be discerned from neuroglia support cells and other native cells by the presence of a thick myelin coating which stained dark blue. Only myelinated axons were used in the evaluation of cord regeneration due to their relative ease in identification and since unmyelinated axons are functionally inconsequential. Digital images of the sections were used for a quantitative analysis of axon geometry.

Images were opened in Adobe Photoshop® where the pen tool was used to trace the myelin sheath around each axon in black. ImageJ software was then utilized to identify each circumscribed axon and measure its perimeter and cross-sectional area. Because cross-sections may have been cut at angles non-orthogonal to axon orientation, many axons did not exhibit a perfect circular shape. The hydraulic diameter was estimated since a true diameter was not able to be evaluated. The hydraulic diameter of an axon is defined as:

$$D_h = (4 \cdot A_{\text{axon}}) / P_{\text{axon}}$$

where  $D_h$  is the hydraulic diameter and  $A_{\text{axon}}$  and  $P_{\text{axon}}$  are the axon area and perimeter, respectively.

The dark blue stain of toluidine blue facilitated the identification of myelin within the regenerated cord. Myelinated axons were found to have crossed into the center of the lesion for all experimental groups. Axons were found to have no typical organization scheme, some were found in small bundles resembling fascicles, with myelinating support cells nearby; others were found in sparsely populated regions. Figure 4.9 shows the total number of axons

populating the middle of the gap lesion for each of the five experimental groups. Values are shown as averages for animals in each group with error bars expressing standard deviations.

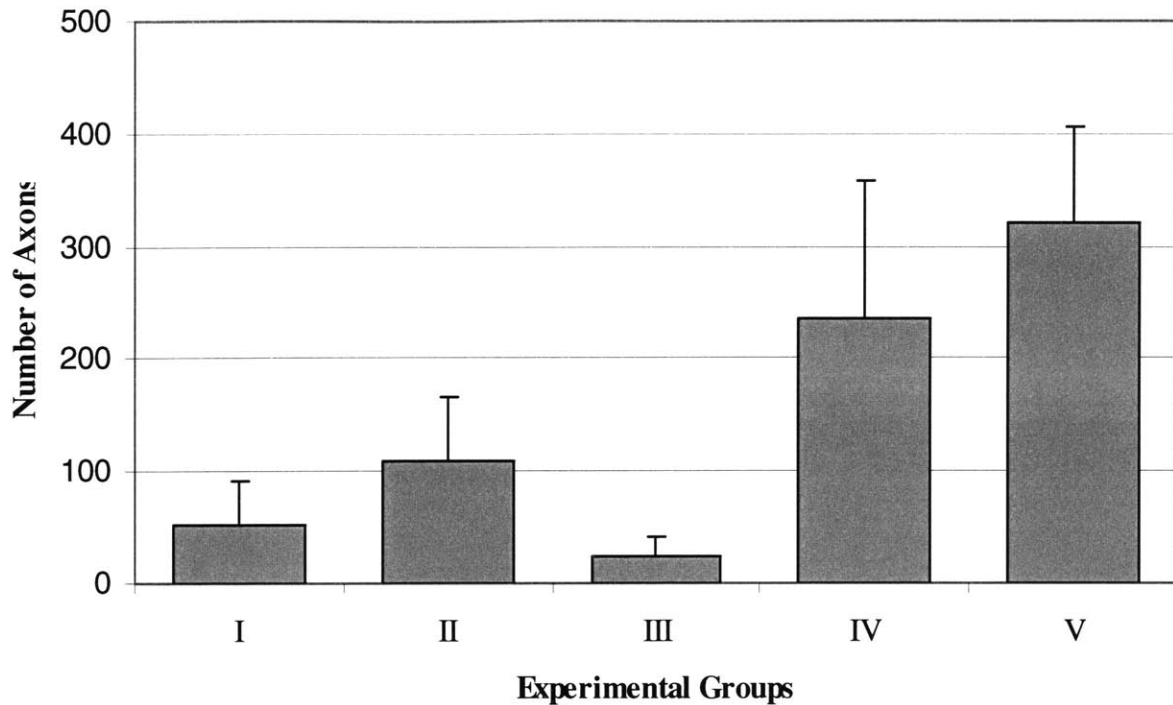


**Figure 4.9** – Number of myelinated axons in the center of the lesion.

Animals of Group V showed the largest number of myelinated axons at the center of the regenerated tissue with  $320 \pm 87$  (mean  $\pm$  SD,  $n=4$ ) myelinated axons. Animals of Group I showed a significantly reduced capacity for axonal regeneration with  $53 \pm 39$  ( $n=3$ ) axons. The placement of the dorsal barrier over the lesion site, Group II, proved some facility at improved axon regrowth with  $110 \pm 55$  ( $n=4$ ) myelinated axons. This trend towards improved axon growth with the use of the dorsal barrier was again seen with Groups III and IV. Animals implanted with the tube alone, Group III, had  $25 \pm 16$  ( $n=4$ ) while the addition of an overlying dorsal barrier, Group IV, improved the myelinated axon count to  $237 \pm 123$  ( $n=4$ ).

A large coefficient of variation was observed across experimental groups suggesting the possibility of non-normally distributed data. It becomes difficult to make firm conclusions based on standard statistical analyses with such distributions. It was decided that care would be taken when evaluating statistical results from a one-way ANOVA and post-hoc tests.



The ANOVA comparison, performed with StatView 5.1, of the myelinated axons found within the center of the lesion illustrated a statistical significance among all experimental groups ( $P = 0.0004$ , Power = 0.998). A post-hoc Fischer's PLSD showed that a comparison between Groups I and IV, I and V, II and IV, and II and V, III and IV and Groups III and V were statistically significant ( $p < 0.05$ ).

As described previously, the hydraulic diameters of axons found in the center of the lesion were measured. The data was compiled as a histogram showing the size distribution of regenerated axons for each experimental group. Figures 4.10 through 4.14 depict the diameter distribution for myelinated axons in each of the five experimental groups. Axon diameters appear to have similar distributions with the majority of axons emerging between one to four microns. Each group exhibited its largest population of axons as two to three microns in diameter.

Figures 4.10 through 4.14 only show the spread of axons up to  $9\mu\text{m}$  in diameter. Individual axons larger than  $9\mu\text{m}$  (and smaller than  $12\mu\text{m}$ ) were found within three experimental groups but composed less than 2% of the total axon population. For the sake of continuity, these outlying values were truncated from the following graphs.

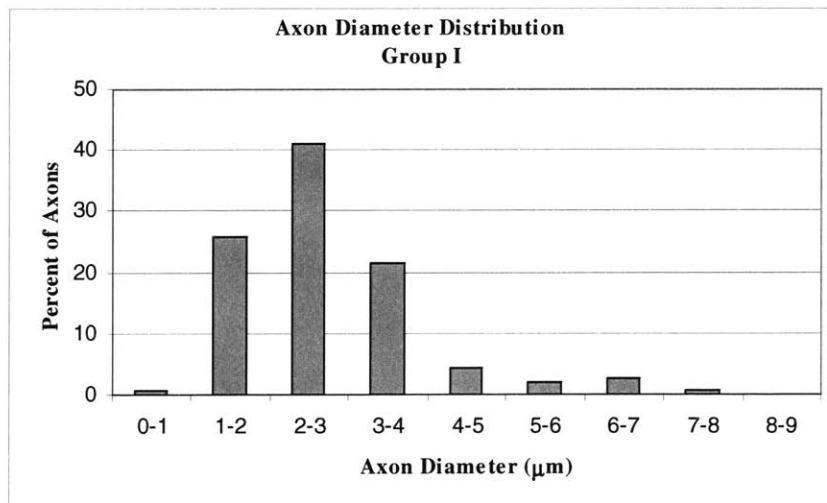


**Figure 4.10** – Distribution of diameters of myelinated axons found in the center of the regenerated tissue for Group I (control)

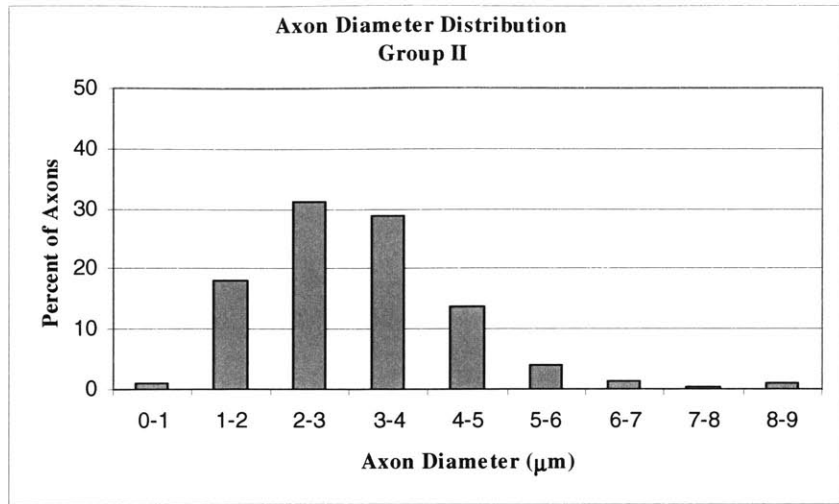


**Figure 4.11** – Distribution of diameters of myelinated axons found in the center of the regenerated tissue for Group II (dorsal barrier)

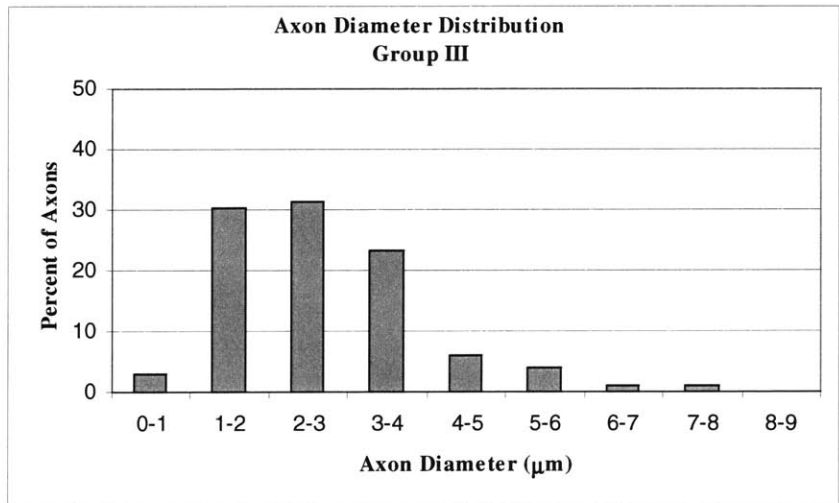


**Figure 4.12** – Distribution of diameters of myelinated axons found in the center of the regenerated tissue for Group III (collagen (5% w/w) tube)

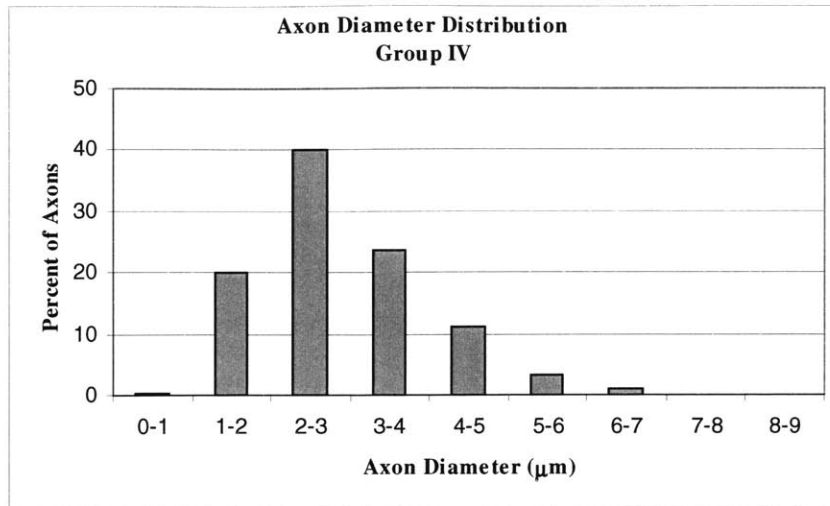


**Figure 4.13** – Distribution of diameters of myelinated axons found in the center of the regenerated tissue for Group IV (tube w/ dorsal barrier)

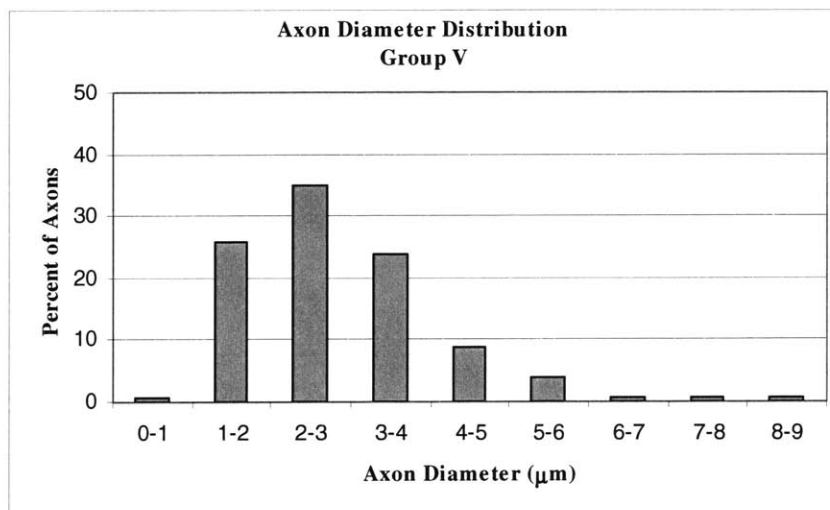


**Figure 4.14** – Distribution of diameters of myelinated axons found in the center of the regenerated tissue for Group V (collagen wrap w/ dorsal barrier)

## Chapter 5: Discussion

The current research aimed at showing the efficacy of collagen based implants towards providing a hospitable environment for axonal regeneration in a spinal cord lesion. The regenerative environment was defined with respect to a chemical analysis of known barriers to competent tissue regeneration and a quantitative analysis of myelinated axons crossing the center of the surgical lesion.

Two implants were defined for the purpose of this research, a collagen (5% w/w) tube and a collagen wrap (made from a commercially available product, BioGide®). The incorporation of a collagen dorsal barrier (also made from BioGide®) into certain experimental groups sought to justify results from a previous study indicating the ability of CG barriers at impeding scar infiltration. Histological, immunohistochemical and quantitative evaluations of explants provided evidence towards the superiority of the collagen wrap to the collagen tube towards promoting axonal regeneration.

The inability of the tube to maintain structural integrity under the pressure of overlying tissue resulted in glial and fibrous scar formation similar to control conditions. The wrap also exhibited deformation induced by loads from overlying tissue. Such loads may cause compression of interior collagen into a denser fibrous barrier. For both implants, the regenerated tissue exhibited noncircular conformations. Future studies should endeavour to evaluate the effect of increased cross-linking density towards improving the mechanical strength of collagen implants. It may also be possible to place a collagenous scaffold within the lumen of the implant to provide structural integrity to the thin-walled tubular implants. Such an inner scaffold may then be seeded with stem cells or growth factors to actively promote nerve regeneration.

The wrap's outer, compact membrane proved sufficiently dense to inhibit scar infiltration while its inner, porous membrane was able to form coherent bonds with regenerative tissue bridging the lesion. The wrap's lumen also exhibited fusion with the tissue of the spinal cord stump after 28 days of implantation. It may be assumed that the ability to form such a cohesive bond shields the delicate regenerating tissue from excessive micro-motion. Such stabilization provides a sound extracellular matrix for axon growth and reduces the likelihood of inflammatory responses. Such was not the case for the tube implant. As

noted earlier, empty spaces extended around the periphery of the regenerated tissue and inhibited the formation of a coherent tissue/implant interface. Fractures along the tube's walls also enabled the infiltration of exogenous soft tissue into the wound environment. Such factors underline the inhospitable regenerative environment elicited by the tube's implantation.

The incorporation of a collagen dorsal barrier proved highly effective towards promoting axon growth. The placement of the dorsal barrier, in many ways, is similar to the concept of the wrap entubulation. By laying a collagen sheet over the lesion, the wound site becomes partially covered, notably secure from overlying musculature and soft tissue. The bed of the vertebral body serves as the bottom half of the entubulated environment. The analyses for each experimental group prove that the dorsal barrier provides an enhanced level of protection from scar infiltration. The dorsal barrier also displayed firm attachment to the spinal stumps (Groups II, IV and V) and regenerated tissue (Group II) which may provide stabilization of the wound and promote axon growth.

The experimental protocol was formulated to abide by the constraints of ethical animal research. It was decided that an additional experimental group, with a wrap implanted without a dorsal barrier, could not be justified. The wrap and dorsal barrier were composed of the same BioGide® membrane. It was assumed that the addition of such a group might prove redundant; that in either case the wound environment would be equally enclosed by the commercially available membrane.

Surgically, the wrap was notably easier to handle and place within the lesion site. Although the collagen tube was manufactured with fixed proportions based on normal rat spinal cord measurements, many cords deviated from those dimensions. It was noted that the surgeon was unable to ensure that the spinal cord stump had been completely ensheathed by the tube implant for cords smaller than expected. The resulting gaps would provide preferential sites for foreign body infiltration and scar formation. For cords larger than expected, the surgeon noted possible secondary trauma induced by forcing the cord stumps into the implant's lumen. Both situations resulted in less than ideal entubulation scenarios at the lesion site. The wrap's flexibility, however, ensured a snug fit and was found to be more amenable to the tight constraints of the lesion's environment.

Clinically, the wrap implant promises to provide a more useful rehabilitative option to spinal cord injury than a tube implant. The vast majority of spinal cord injuries are the result of blunt trauma. Partial paralysis, where portions of the spinal cord remain intact and functional, is more likely to result from such trauma than complete paralysis. Although the current research focused on complete paralysis induced by transection, it is evident that the ensheathment technique afforded by the collagen membrane could work equally well in hemisection or crushing (i.e. partial paralysis) experiments.

Proper implantation of the preformed tubular implant necessitates the complete transection of the spinal cord. Few clinicians, if any, would advocate the removal of functional cord tissue based on the optimistic hopes of regenerative tissue engineering. Ensheathment promises to be a more practical method for maintaining wound isolation and managing local environmental factors.

## Chapter 6: Conclusions

The current research established a set of qualitative criteria to evaluate the local environment of a healing spinal cord lesion. The absence of glial and fibrous scar was directly associated with the improved capacity for axonal regeneration. The degree of axon regeneration was defined by the gross number and diameter of myelinated axons able to penetrate the middle of the gap lesion.

The mechanical loads of overlying musculature and soft tissue were shown to cause buckling fractures in tube implants and compressive deformations to the wrap implant. It became evident that a tubular implant, alone, may not provide sufficient protection from the physiological and anatomical environments. Based on the criteria established, it was found that the collagen wrap implant (Group V) proved most successful. The presence of myelinated axons within the lesion proved encouraging, as did the incorporation of a dorsal barrier towards wound stabilization and scar inhibition.

The current research has shown the promise of utilizing collagen sheets to entubulate spinal cord lesions. Future research should hope to optimize the inherent strengths and buttress known weaknesses of these sheets towards facilitating functional recovery following trauma to the spinal cord.

## Appendix A

### 5% Collagen Tube Fabrication Protocol

(adapted from Harley 2002)

#### *Supplies*

0.25 gm Type I Collagen  
150  $\mu$ l Glacial Acetic Acid  
10 ml Degassed, Distilled Water [ddH<sub>2</sub>O]

#### *Procedure*

1. Degas 10 ml distilled water for 10-15 minutes.
2. In centrifuge tube, mix 150  $\mu$ l Glacial Acetic Acid with 850  $\mu$ l ddH<sub>2</sub>O, forming 3.0M acetic acid. Draw solution into 3 ml syringe with 22 gauge needle (Cat. No. 309574, Beckton Dickinson & Co., Franklin Lakes, NJ).
3. Weigh 0.25 g Type I Collagen (Integra Life Sciences, San Diego, CA). Place collagen into 10 ml syringe (Cat. No. 309604, Beckton Dickinson & Co., Franklin Lakes, NJ) that has Parafilm covering luer-lock end. Add 4 ml ddH<sub>2</sub>O and mix thoroughly with forceps.

Insert plunger into syringe and invert syringe, allowing collagen mixture to fall away from the syringe tip. Remove Parafilm and mix collagen slurry by moving stopper up and down. Plunge air out from tip, bringing plunger up so that slurry comes up to the tip.

4. Slowly inject 1 ml 3.0M acetic acid into collagen, placing the needle from the 3 ml syringe through the tip of the 10 ml syringe with collagen-water suspension. Add the 1 ml acetic acid slowly while mixing with needle tip and pulling back on the 10 ml syringe plunger.
5. Blend slurry well until a homogeneous mixture is achieved. Attach 10 ml syringe with collagen slurry to another 10 ml syringe with a female-female Luer-lock assembly (Stainless steel luer lock tube fitting, female luer x female luer, Cat. No. 5194k12, McMaster-Carr Supply Company, New Brunswick, NJ) and mix by injecting collagen slurry from one syringe to another. Mix back and forth 10-15 times, until collagen fibers begin to hydrate and solution appears uniform.
6. After mixing, remove empty syringe and Luer-lock fitting. Cover syringe tip with multiple layers of Parafilm to seal the syringe so that the collagen does not escape during centrifugation.

Do not remove plunger, let slurry mixture sit for 3 hours at room temperature to allow for the collagen fibers to swell.

After 3 hours, remove plunger, but keep Parafilm over syringe tip.

7. Set Freeze-Drier to -40°C



8. Centrifuge the collagen slurry in the syringe in order to degas the collagen so that a homogeneous collagen slurry without any macroscopic air bubbles forms. Place the syringe into a 50 ml conical tube, using paper towel to brace the syringe along the central axis of the conical tube. Centrifugation should be done at 4500 rpm (maximum angular velocity) at 25°C for 60 minutes (Heraeus Labofuge 400R). This angular velocity translates to 3940G
9. Inject centrifuged (degassed) collagen slurry into Teflon mold. Inject slurry into closed molds until slurry is apparent on other side. Insert quartz mandrel (coated with Teflon tubing) into the slurry, rotating the mandrel during insertion so as to keep the mandrel centered and to maintain a uniform deposition of collagen throughout the mold. Cap the ends of the mandrel with the centering tubes after the mandrel is fully inserted.
10. Place molds in freeze-drier for 1 hour at -40°C.
11. Pull vacuum in freeze-drier until interior pressure reads below 100 mTorr.
12. Raise temperature to 0°C and leave the mold in the vacuum freeze-drier overnight (17 hours)
13. Raise temperature to 20°C and release vacuum
14. Gently open molds and remove tubes.

## Appendix B

### The Teflon Mold

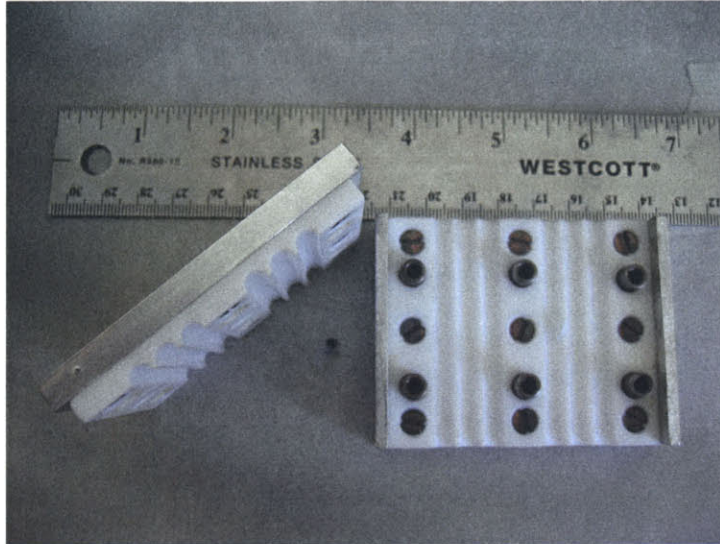


**Figure B.1** – The mold was encased in an aluminum shell to provide structural rigidity to the Teflon. Six holes (3.3 mm in diameter) were milled down the central portion of the mold, which breaks into two halves allowing easy access to freeze-dried tubes.

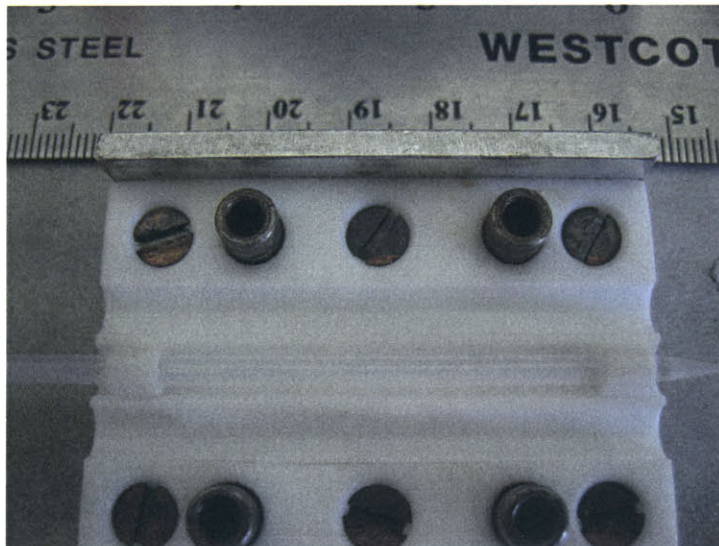


**Figure B.2** – A quartz rod was fitted into a thin Teflon tube creating a mandrel of 3.0mm in diameter. In order to ensure that the mandrels rested securely and centrally within each hole, spacers were made (ID – 3.0mm, OD – 3.3mm).

## References

### Works Cited

- Basso, D. M., M. S. Beattie, et al. (1996). "Histological and locomotor studies of graded spinal cord contusion using the NYU weight-drop device versus transection." Experimental Neurology **139**: 224-256.
- Beattie, M. S., J. C. Bresnahan, et al. (1997). "Endogenous repair after spinal cord contusion injuries in the rat." Experimental Neurology **148**: 453-463.
- BioGide (2004). BioGide® product information available from <http://www.geistlich.com>.
- Blesch, A., Lu, P., et al. (2002). "Neurotrophic factors, gene therapy, and neural stem cells for spinal cord repair." Brain Research Bulletin **57**(6): 833-8.
- Blight, A. R. and V. Decrescito (1986). "Morphometric analysis of experimental spinal cord injury in the cat: the relation of injury intensity to survival of myelinated axons." Neuroscience **19**: 321-341.
- Bregman, B. S., Kunkel-Bagden, E., Schnell, L., Dai, H.N., Gao, D., and Schwab, M.E. (1995). "Recovery from spinal cord injury mediated by antibodies to neurite growth inhibitors." Nature (London) **378**: 498-501.
- Burke, J. F., Yannas, I.V., Quinby, W.C., Bondoc, C.C., and Jung, W.K. (1981). "Successful use of a physiologically acceptable artificial skin in the treatment of extensive burn injury." Annals of Surgery **194**: 413-428.
- Chamberlain, L. J., Yannas I.V. (1998). Preparation of collagen-glycosaminoglycan copolymers for tissue regeneration. Methods in Molecular Medicine: Tissue Engineering

Methods and Protocols. J. R. Morton, Yarmush, M.L. Totowa, NJ, Humana Press. Vol 20: pp3-17.

Chen, A., Xu, X.M., Kleitman, N., and Bunge, M.B. (1996). "Methylprednisolone administration improves axonal regeneration into Schwann cell grafts in transected adult rat thoracic spinal cord." Experimental Neurology **138**: 261-276.

Clemente, C. D. a. W., W.F. (1954). "Regeneration of severed nerve fibers in the spinal cord of the adult cat." Journal of Comparative Neurology **101**: 691-731.

David, S., Aguayo, A.J. (1981). "Axonal elongation into peripheral nervous system "bridges" after central nervous system injury in adult rats." Science **214**: 931-3.

Davies, S. J. A., Fitch, M.T., Memberg, S.P., Hall, A.K., Raisman, G., and Silver, J. (1997). "Regeneration of adult axons in white matter tracts of the central nervous system." Nature **390**: 680-683.

Fitch, M. T., Silver, J. (1999). Beyond Glial Scar. CNS Regeneration. M. H. a. K. Tuszynski, J., Academic Press.

Grill, R. J. a. T., M.H. (1999). Axonal Responses to Injury. CNS Regeneration. M. H. a. K. Tuszynski, J., Academic Press.

Guth, L., C. P. Barrett, et al. (1985). "Essentiality of a specific cellular terrain for growth of axons into a spinal cord lesion,." Experimental Neurology **88**: 1-12.

Guth, L. B., C.P., Donati, E.J., Anderson, F.D., Smith, M.V., and Lifson, M. (1985). "Essentiality of a specific cellular terrain for regrowth of axons into a spinal cord lesion." Experimental Neurology **88**: 1-12.

Harley, B. A. (2002). Peripheral nerve regeneration through collagen devices with different in vivo degradation characteristics. Cambridge, MA, Massachusetts Institute of Technology.

Harley, B. A., Spilker, M.H., Wu, J.W., Asano, K., Hsu, H.-P., Spector, M., Yannas, I.V. (2004). "Optimal degradation rate for collagen chambers used for regeneration of peripheral nerves over long gaps." Cells, Tissues, Organs **176**: 153-165.

Heimbach, D., Luterman, A., Burke, J., Cram, A., Herndon, D., Hunt, J., Jordan, M., McManus, W., Solem, L., Warden, G., and Zawacki, B. (1988). "Artificial dermis for major burns." Annals of Surgery **208**: 313-320.

ICCP (2000). from an information package provided by the International Campaign for Cures of Spinal Cord Injury Paralysis.

Institute of Laboratory Animal Resources (1996). Guide for the use and care of laboratory animals. Washington, DC, National Academic Press.

Kandel, E. R., Schwartz J.H., Jessell T.M. (2000). Principles of Neural Science. New York, NY., McGraw-Hill.: 1108-1110.

Kiernan, J. A. (1979). "Hypotheses concerned with axonal regeneration in the mammalian nervous system." Biological Review **54**: 155-197.

Krikorian, J. G., Guth, L., and Donati, E.J. (1981). "Origin of the connective tissue scar in the transected rat spinal cord." Experimental Neurology **72**: 698.

Liu, H. M. (1981). Biology and Pathology of Nerve Growth, Academic Press.

McDonald, J. W. (1999). "Repairing the damaged spinal cord." Scientific American **281**(3): 64-73.

Menei, P., Montero-Menei, C., Whittemore, S.R., Bunge, R.P., and Bunge, M.B. (1998). "Schwann cells genetically modified to secrete human BDNF promote enhanced axonal regrowth across transected adult rat spinal cord." European Journal of Neuroscience **10**: 607-621.

Midha, R., M. G. Fehlings, et al. (1987). "Assessment of spinal cord injury by counting corticospinal and rubrospinal neurons." Brain Research **410**: 299-308.

Nicogossian, A. (2000). Hearing of the Subcommittee on Space and Aeronautics, US House of Representatives.

Oudega, M. V., C.G., Weber, A.B., Kleitman, N. and Bunge, M.B. (1999). "Long-term effects of methylprednisolone following transection of adult rat spinal cord." European Journal of Neuroscience **11**: 2453-2464.

Pinzon, A., Calancie, B., et al. (2001). "Conduction of impulses by axons regenerated in a Schwann cell graft in the transected adult rat thoracic spinal cord." Journal of Neuroscience Research **64**(5): 533-41.

Ramon y Cajal (1928). Degeneration and Regeneration of the Nervous System. London, UK, Oxford University Press.

Rudge, J. S., Smith, G.M., Silver J. (1989). "An in vitro model of wound healing of the CNS: analysis of cell reaction and interaction at different ages." Experimental Neurology **103**: 1-16.

Savio, T. a. S., M.E. (1989). "Rat CNS white matter, but not gray matter, is nonpermissive for neuronal cell adhesion and fiber outgrowth." Journal of Neuroscience **9**: 1126 1133.

Schwab, M. E. (1990). "Myelin-associated inhibitors of neurite growth and regeneration in the CNS." Experimental Neurology **109**: 2-5.

Schwab, M. E. a. C., P. (1988). "Oligodendrocytes and CNS myelin are nonpermissive substrates for neurite growth and fibroblast spreading in vitro." Journal of Neuroscience **8**: 2381-2393.

Smith, G. M., Rutishauser, U., Silver, J., Miller, R.H. (1990). "Maturation of astrocytes in vitro alters the extent and molecular basis of neurite outgrowth." Developmental Biology **138**: 377-390.

Sofroniew, M., V. (1999). Neural Responses to Axotomy. CNS Regeneration. T. M. H. a. K. J, Academic Press.

Spilker, M. H. (1997). The effect of porous collagen-glycosaminoglycan matrix on healing of the injured rat spinal cord. Cambridge, MA, Massachusetts Institute of Technology.

Spilker, M. H. (2000). Peripheral nerve regeneration through tubular devices: A comparison of assays of device effectiveness. Cambridge, MA, Massachusetts Institute of Technology.

Spilker, M. H., Yannas, I.V., et al. (2001). "The effects of tubulation on healing and scar formation after transection of the adult rat spinal cord." Restor Neurol Neurosci **18**(1): 23-38.

Stokes, B. T. and P. J. Reier (1991). "Oxygen transport in intraspinal fetal grafts: graft-host relations." Experimental Neurology **111**: 312-323.

Stone, K. R., Rodkey, W.R., Webber, R.J., McKinney, L., and Steadman, J.R. (1990). "Future directions: collagen-based prostheses for meniscal regeneration." Clinical Orthopaedic and Related Research **252**: 129-135.

Theriault, E. and C. H. Tator (1994). "Persistence of rubrospinal projections following spinal cord injury in the rat." Journal of Comparative Neurology **342**: 249-258.

Tuszynski, M. H., Weidner, N., McCormack, M., Miller, I., Powell, H., and Conner, J. (1998). "Grafts of genetically modified Schwann cells to the spinal cord: Survival, axon growth, and myelination." Cell Transplant **7**: 187-196.

Vacanti, M. P., Leonard, J.L. (2001). "Tissue-engineered spinal cord." Transplant Proc **33**(1-2): 592-8.

Wickelgren, I. (2002). "Animal studies raise hopes for spinal cord repair." Science **297**(5579): 178-181.

Windle, W. F. a. C., W.W. (1950). "Regeneration in the spinal cord of the cat and dog." Journal of Comparative Neurology **218**: 460-470.

Yannas, I. V. (1981). Chapter 15: Use of artificial skin in wound management. The Surgical Wound. (Ed) P. Dineen. Philadelphia, PA. Lea and Febiger.

Yannas, I. V., Lee, E., Orgil, D.P., Skrabut, E.M., Murphy G.F. (1989). "Synthesis and characterization of a model extracellular matrix that induces partial regeneration of adult mammalian skin." Proc Natl Acad Sci, USA **86**: 933-937.

Yannas, I. V., Orgill, D.P., Silver, J., Norregaard, T.V., Zervas, N.T., and Schoene, W.C. (1987). Regeneration of sciatic nerve across 15mm gap by use of a polymeric template. Advances in Biomedical Polymers. (Ed) C. G. Gebelein. New York, NY. Plenum Publishing.

Yannas, I. V., Tobolsky, A.V. (1967). "Cross-linking of gelatin by dehydration." Nature **215**(509-510).



## Sources for Certain Figures

Figure 1.1 – Berne, R.M., Levy, M.N. (1998). Physiology. St. Louis, MO. Mosby. p87.

Figure 1.2 – Kandell, E. R., Schwartz J.H., Jessell T.M. (2000). Principles of Neural Science.  
New York, NY., McGraw-Hill. pp1108-1110.

Figure 1.3 - Berne, R.M., Levy, M.N. (1998). Physiology. St. Louis, MO. Mosby. p94